Kasandra Escárcega Herrera
Candidate
Mechanical Engineering
Department

This thesis is approved, and it is acceptable in quality and form for publication:

Approved by the Thesis Committee:

Custom Cathode Optimization for Electropolishing Additively Manufactured 316L Stainless Steel

by

Kasandra Escárcega Herrera

B.S. in Mechanical Engineering, The University of New Mexico, 2023

THESIS

Submitted in Partial Fulfillment of the
Requirements for the Degree of

Master of Science

Mechanical Engineering

The University of New Mexico
Albuquerque, New Mexico

May, 2025

DEDICATION

Dedico mi trabajo de titulación a mi familia, que gracias a ellos y su apoyo fué possible alcanzar este logro. Mi Papá, mi Mamá, y mi hermano fortalecieron el amor por el aprendizaje y me enseñaron el valor de la educación. Sus propios logros personales han sido una gran motivación e inspiración para mí. Gracias por ayudarme a encontrar la felicidad y humor en cada situación. Realmente aprecio sus sacrificios y cargo su valtentía conmigo en todo momento.

I dedicate this project to my family who helped make this journey possible. To my dad, mom, and brother who strengthened my love for learning and taught me the importance of education. Your own accomplishments have been my greatest source of motivation and inspiration. Thank you for helping me find the joy and humor in every situation. I truly value your sacrifices and I carry your strength with me every step of the way.

ACKNOWLEDGMENTS

This work would not have been possible without the guidance, expertise, and patience of my mentor, Dr. Michael Melia. Thank you for trusting me with this project, I am grateful for your constant encouragement. Your support has been instrumental to my growth. Thanks to my manager, Dr. Nicholas Wyatt, for ensuring that his team is always well taken care of. Thank you to Dr. Mary Louise Gucik for her endless support, wisdom, and the much-needed laughter. Thank you to Mr. Jason Taylor for encouraging me to think outside the box with his reliable and creative solutions. Thank you to Dr. Erin Karasz for her years of endless guidance, encouragement, and support. Thank you to Dr. Peter Renner for encouraging me to push myself and pursue difficult challenges. Thank you to Dr. Yu-Lin Shen and Dr. Pankaj Kumar for sparking my scientific curiosity and serving on my thesis committee. I would also like to thank David Saiz for providing the material and printers that made this research possible. Thank you to our collaborators Dr. Jamie Stull and Dr. Alex Mirabal for their contributions. I am appreciative of everyone that contributed their support to help make this project possible.

Research was conducted at Sandia National Laboratories. Sandia National Laboratories is a multimission laboratory managed and operated by National Technology & Engineering Solutions of Sandia, LLC, a wholly owned subsidiary of Honeywell International Inc., for the U.S. Department of Energy's National Nuclear Security Administration under contract DE-NA0003525.

Custom Cathode Optimization for Electropolishing Additively Manufactured 316L Stainless Steel

by

Kasandra Escárcega Herrera

B.S., Mechanical Engineering, The University of New Mexico, 2023

M.S., Mechanical Engineering, University of New Mexico, 2025

Abstract

Laser powder bed fusion (LPBF) has become increasingly popular for its ability to rapidly manufacture complex metallic parts. However, the surface properties of as-built LPBF parts may degrade overall performance due to tortuous surface features. Consequently, post-processing like electropolishing (EP) to reduce the surface asperities is often needed for LPBF parts to perform as expected. Utilizing experimental and computational approaches, this project aims to more uniformly EP complex shaped parts made from LPBF 316L. For the experimental approach, parts with a three-dimensional T-shape were printed out of 316L stainless steel and EP using an acidic-based and a polyethylene glycol/NaCl-based electrolyte. A series of cathodes were designed to show how the uniformity of material removal across the T-shaped parts entire surface varies when different combinations of electrolyte, cathode, and electrode spacing were used in the EP process. The first three cathodes tested had a flat, cylindrical, and conformal shape, each with two different electrode spacings (2 and 20 mm). The results from the experiments using different cathode shapes were then compared to a COMSOL model designed to capture the impact of cathode shape on material removal. Based on those results, a cathode was then optimized using COMSOL, designed in Solidworks, printed out of LPBF 316L, and used to polish an anode selectively and uniformly. Based on all the metrics tested before and after EP; mass loss, surface roughness, reflectivity, and local thickness removal from 3D optical scans, the selective cathode performed the best compared to the other cathodes. The relationship between cathode shape and uniformity of material removal across the entire T-shaped parts surface will be discussed in depth.

Table of Contents

List of Figures

List of Tables

Chapter 1 – Introduction

Metal additive manufacturing (AM) is a technology capable of creating incredibly complex parts. In general, AM processes create parts by depositing material in a layer-by-layer fashion based on a computerized 3D model. In contrast, traditional manufacturing techniques typically employ subtractive manufacturing methods in which a large ingot of metal is machined into its final form. One of the advantages of the AM process is the ability to create complex parts with features that would otherwise be difficult to create through traditional manufacturing methods, such as lattices, resulting in increased design flexibility and in some cases functionality [2]. Additionally, AM processes can reduce material waste in comparison to traditional subtractive manufacturing techniques [3]. Another advantage is the ability to prototype parts rapidly which can be both time and cost-effective. The AM process has become a common tool in several industries, including aerospace, automotive, and medical [4].

Although AM offers a variety of advantages, it also presents challenges as metal AM in particular makes parts with as-built surfaces that are highly tortuous [2-4]. Several factors, contribute to the increased surface roughness and heterogeneous microstructures inherent to the AM process. These surface morphologies, microstructures, and internal stresses include the stair-step effect, partially fused particles, porosity, and residual stresses among others [2]. Untreated AM parts typically exhibit issues in terms of corrosion and fatigue behaviors, which are detrimental to part life and reliability [3]. As a result, as-printed (AP) metallic AM parts typically require post-processing to remove these surface defects and internal stresses [4].

Surface treatments are available to smooth AM surfaces, including mechanical polishing, media blasting, chemical polishing, and electropolishing. Electropolishing stands out as a particularly effective post-processing treatment, as it removes surface impurities without inflicting additional mechanical stresses. Electropolishing is also capable of polishing parts with complex geometries that would otherwise be inaccessible through other surface finishing techniques. However, there is limited research on the intricacies of the electropolishing process, with even less publications on AM parts [4].

Electropolishing is highly dependent on several factors such as electrolyte composition, electrode spacing, and cathode geometry, yet there is limited research on these topics. Typically, metallic parts are electropolished using strong acids, which are hazardous, and few studies have investigated alternative, environmentally friendly electrolytes. A study conducted by Ferreri et al., successfully developed a procedure to electropolish titanium samples using an alternative ethanol-ethylene glycol-NaCl (sodium-chloride) electrolyte [5]. Another study by Han and Fang compared a conventional acid-based electrolyte to an alternative NaCl-based electrolyte for electropolishing 316L stainless steel and found that both produced comparable results [6].

Electrode spacing, the distance between the anode (the part) and cathode (supplying electricity), is known to influence current density distributions across the anode's surface [7]. Lassel conducted a study electropolishing AM Ti-6Al-4V with electrode spacings of 5, 7.5, and 10 mm and found that as the electrode gap reduced, so did the resultant surface roughness [8]. Other work by Chaghazardi shows 316L stainless steel tubes exhibited a significant improvement in surface brightness the smaller the

electrode spacing gets (the smallest gap being 1 mm) [9]. No work could be found on electrode gaps smaller than 0.5 mm.

To date, there are few studies investigating the impact of cathode geometry on electropolishing results, as most employ flat or cylindrical cathode geometries [7, 8, 10, 11]. One study by Lynch et al. successfully electropolished an AM Inconel 718 cubic lattice with a slotting cathode assembly, achieving up to a 70% reduction in surface roughness on the internal lattice anode [12].

The current research was undertaken to determine how varying electrolyte composition, electrode spacing, and cathode geometry impact electropolishing of LPBF 316L stainless steel. The electrolytes chosen for this study were a conventional acid-based electrolyte and an environmentally friendly NaCl-PEG-based electrolyte. Electrode spacing ranged from 2 mm to 20 mm. Cathode geometries with increasing conformity, consisting of a flat, cylindrical, and conformal cathode, were compared. Electropolishing results were quantified through surface roughness, mass change, visible light reflectivity, optical imagery, and 3D profilometry. Additionally, a COMSOL model was developed to inform cathode design to increase overall uniformity of material removal across the entire surface. The optimized cathode was tested and potential improvements to this optimization process will be discussed.

1.1: Background

There are several different AM techniques. Among the most prominent is Fused Deposition Modeling (FDM) in which a thermoplastic polymer is heated and extruded in a layer-by-layer fashion. Stereolithography is one of the earliest AM techniques in which a UV light is used to cure layers of resin or monomer into a desired shape. Directed Energy Deposition is a technique in which an energy source (typically a laser or electron beam) fuses material by melting the substrate as it is deposited.

Laser Powder Bed Fusion (LPBF) is one of the most common techniques used to create metallic parts. LPBF uses a high-powered laser to selectively melt and fuse thin layers of powder onto a build plate. Subsequent powder layers are rolled over the existing layers and fused together, rapidly solidifying to form the part/parts as dictated by the computerize 3D design [13]. LPBF results in significant temperature gradients, because the melt pool created by the laser is liquid for fractions of a second, resulting in cooling rates on the order of 100,000 K/sec. Large temperature gradients generate fine-grained, anisotropic microstructures that are far from equilibrium and can cause considerable residual stresses to develop in parts.

1.1.1: Surface Morphology of AM Parts

AM surfaces are notorious for having heterogenous microstructures that influence their performance. One of the biggest challenges with AM parts is the large surface roughness which can be attributed to the stair-step effect, partially fused particles, and porosity. Residual stresses, generated by rapid heating and cooling during the LBPF, can lead to distortions and fractures if able to exceed the yield or ultimate tensile strength of

the material. The following section describes in detail how these defects form on AM parts [4].

1.1.2: Stair-step Effect

LBPF processes typically produce AP parts with high surface roughness which can be attributed to various factors inherent in the process. Among these factors is the stair-step effect. As material is deposited layer by layer, the edges create a stepped appearance when one layer is deposited slightly offset from the previous layer. This becomes particularly prominent on curved or inclined surfaces, thereby contributing to surface roughness [14, 15]. Similar effects are seen on the "top" surface of a part where melt pools are deposited next to each other creating a periodic surface morphology dictated by the hatch spacing of the melt pools. Both the hatch spacing, and layer height are critical to defining the amplitude of the periodic surface morphology and contribute directly to the waviness portion of the surface roughness measurement.

One method of reducing the effect is by decreasing the layer thickness, which leads to longer build times and increased cost. Another alternative is to reduce powder particle size; however, finer powders tend to be more expensive and can cause other issues like poor chemistry control or they become more hazardous to work with [16]. Reducing slope angle has been thought to reduce surface roughness. However, Strano et al. conducted a study investigating the effect of slope angle on the surface roughness of 316L stainless steel parts made by LPBF and found minimal correlation. At slope angles between 5°-45°, surface roughness was 16 μm. On highly sloped surfaces between 80°-90°, surface roughness was expected to be minimal; however, it was measured to be 14 μm which did not differ significantly from the roughness of lower sloped angles [15].

1.1.3: Partially Fused Particles

Several studies agree that partially fused particles are a significant factor contributing to the increased finer scale surface roughness features found on LPBF parts [4, 15, 17-22]. These parts often contain sharp, high aspect ratio features formed through the partial melting and adhesion of powder particles on the outermost edge (Figure 1) [17]. The study by Strano et al. analyzed LBPF samples through scanning electron microscopy (SEM) and found that partially fused particles were responsible for increased surface roughness. It was also observed that as the slope angle increased, a larger density of partially fused particles was found along the step edges. This is believed to be caused by insufficient heat at the edge borders, not adequate to completely melt the powder particles [15]. Another study by Melia et al. concurs that surface roughness is influenced by the amount of partially fused particles, which is dependent on build angle for a LPBF 316L stainless steel part printed with a parallelepiped prism shape. Surfaces with larger build angles (>90^{o} – overhanging features) were shown to exhibit larger roughness values, attributed to partially fused particles, when compared to surfaces with smaller build angles (<90^{o} – upward facing surfaces) [17].

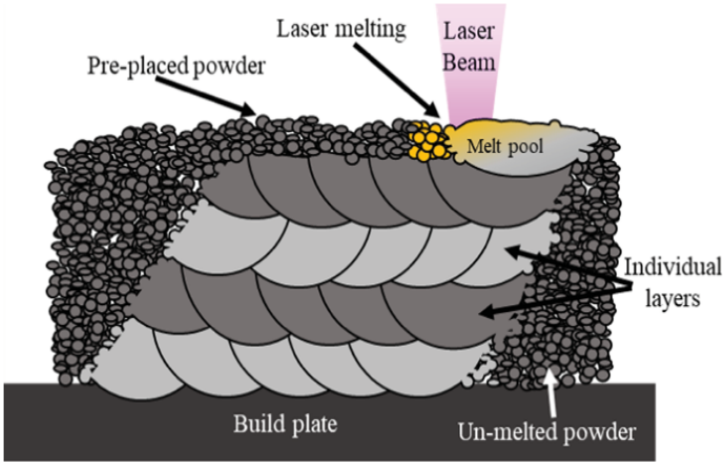

Figure 1. Cross-sectional schematic of the LPBF process (Melia et al., 2020).

1.1.4: Porosity

SLM techniques, like LPBF, often result in porous parts due to the absence of mechanical pressure during the process [4]. Liu and Shin have reported porosity values in SLM parts to range from approximately 0.1 to 0.5 vol% [23]. Benedetti and Morgan et al. have attributed this porosity to several factors, including powder contaminants, gas bubble entrapment during solidification, and insufficient fusion of thicker areas of powder layers due to inadequate laser energy and surface roughness from previous layers [24]. Chaghazardi claims that the static and dynamic strengths of the part are reduced due to these porosities, as they reduce the overall load-bearing area. Porosities act as stress concentration sites which enable crack initiation. They also influence corrosion susceptibility as they promote early pitting [4].

1.1.5: Residual Stresses

The rapid heating and cooling inherent to the SLM process results in the retention of thermal and residual stresses within the material. Chaghazardi attributes different phases present in the microstructure and dislocations in the material as significant contributors to microscopic residual stresses observed in AM parts [4]. Vayssette et al. compared residual stresses between two techniques: LPBF and E-beam powder bed fusion (PBF). E-beam PBF parts were reported to have very low residual stress values in comparison to SLM parts, which ranged between 100-500 MPa [25]. AM parts can become distorted or fractured if residual stresses reach and surpass the material's yield strength [4]. Residual stresses are known to increase material brittleness and reduce part strength [26-28]. When combined with porosity, residual stresses can also lead to stress corrosion cracking [4]. Overall, residual stresses significantly compromise the

mechanical behavior of AM parts; future sections will discuss methods to mitigate these effects.

1.1.6: 316L Stainless Steel

Stainless steels, and especially 316L stainless steels, are known for their enhanced corrosion resistance and mechanical properties. 316L is typically composed of iron, 16-18% chromium, 10-14% nickel, and 2-3% molybdenum. The material obtains "stainless" qualities as the chromium forms a passive oxide layer which aids in the prevention of corrosion. 316L stainless steel produced through traditional manufacturing techniques, including casting and forging, typically has a homogeneous microstructure. In contrast, 316L stainless steel produced through AM techniques oftentimes exhibits unique surface morphologies that impact mechanical properties and performance [29].

1.2: Impact of AM Microstructure on Mechanical Properties

Surface roughness and microstructure heterogeneities significantly impact the mechanical properties of AM surfaces, particularly in terms of fatigue behavior and environmentally assisted cracking. Rough AM surfaces are more susceptible to corrosion as they provide a larger area and more potential sites for corrosion initiation. Surface defects such as partially fused particles and non-metallic inclusions act as stress concentrators, affecting the fatigue life of AM parts. The following section will detail the impact of AM microstructures on mechanical behaviors.

Several studies have demonstrated that surface roughness significantly influences the corrosion resistance of a part [4, 17, 30-34]. Some studies have suggested that heterogeneities in AM microstructures, such as partially fused particles and non-metallic inclusions, act as corrosion initiation sites, and that reducing these heterogeneities results

in enhanced corrosion resistance [35, 36]. One study conducted by Melchers et al. investigated the effect of surface finish on marine immersion corrosion exposures. The findings revealed that surface finish significantly influenced corrosion rates, especially during the early weeks of exposure. The study attributed this effect to the fact that surfaces with greater surface roughness have a larger overall area susceptible to corrosion [4, 34]. Another study by Melia et al. investigated how surface roughness affected corrosion initiation and susceptibility of AM 316L stainless steel surfaces in a 0.6M NaCl solution. The study found that surface roughness and partially fused features are major contributors to passivity breakdown, indicating that rougher AM metal surfaces have an increased susceptibility to corrosion. The results also found that polished samples with the greatest reduction in surface roughness performed best, exhibiting statistically larger (p-value < 0.05) breakdown potential values when compared to as-printed surfaces [17]. These results were confirmed by a study conducted by Cabrini et al., which investigated the effect of surface finish on the corrosion resistance of AM Al-Si10-Mg surfaces [37]. The results demonstrated that the corrosion resistance of these surfaces increased significantly after shot peening and polishing, especially when compared to unpolished surfaces [37].

Porosity has also been shown to influence corrosion susceptibility of an AM part. Sander et al. conducted a study on SLM 316L austenitic stainless steel samples, examining the relationship between porosity to cyclic polarization as well as pitting behaviors. The results concluded that samples with higher porosity experienced a greater frequency of metastable pitting. Additionally, the results demonstrated that repassivation potential decreased as sample porosity increased [36].

It is well understood that fatigue properties are primarily affected by surface roughness and porosity [4, 38-40]. A study conducted by Wycisk et al. analyzed the mechanical characteristics of AM Ti-6Al-4V. The results indicated that the endurance limit of polished AM surfaces increased from 210 MPa to 500 MPa in comparison to as-printed AM surfaces. The authors attributed the increase in endurance limit to the reduction of surface roughness and defects presents on AM surfaces [38]. Another study conducted by Chan et al. corroborated the influence of surface roughness on fatigue behavior between AM and rolled Ti-6Al-4V. The results demonstrated that rough AM samples exhibited a significantly lower ($p < 0.05$) fatigue life when compared to the smoother rolled material [41].

Although, surface roughness is a significant factor influencing fatigue behavior, it is not the only one [4, 38-40]. Edwards et al. demonstrated that as rough surfaces are polished, underlying porosity is exposed. These porosities can accelerate the premature failure of a part. The study concluded that while surface roughness significantly affects fatigue behavior, special caution must be exercised when polishing these surfaces, as underlying porosity can create stress concentration sites for crack initiation [42]. Another study by Wycisk et al. examined crack initiation in AM Ti-6Al-4V samples. The results indicated that, on as-printed surfaces, cracks initiated on the outer surface and progressed inward. However, on polished surfaces, cracks initiated both on the outer surface and at interior pores [4, 38].

1.3: Post-Processing Treatments

Post-processing is a crucial step in the production of AM parts when failure risk is needed to be minimized [4]. Numerous studies [4, 17, 30-34, 37, 38, 41-43] have

demonstrated that removing defects on AM surfaces through polishing techniques have significantly enhanced mechanical and corrosion properties, highlighting the importance of post-processing AM surfaces. The following section will discuss post-processing techniques, such as heat treatments and polishing, which are necessary to remove these defects.

1.3.1: Heat Treatments

Heat treating AM samples has been demonstrated to improve mechanical performance [4]. Brandl et al. investigated the effects of peak hardening on the microstructure and mechanical properties of AM Al-Si10-Mg surfaces. The results indicated that peak hardening significantly increased the Weibull constants corresponding to fatigue limit and tensile strength, thereby enhancing the fatigue resistance [44]. Another study by Song et al. examined the effect of heat treatment under vacuum on AM iron parts. The results demonstrated that the annealing heat treatment process relieved residual stresses, led to grain refinement, and increased both yield strength and ultimate tensile strength [45].

Another approach to heat treating is through hot isostatic pressing (HIP), which combines the use of high temperatures and pressures. Several studies have shown that HIP reduces and even closes pores on AM surfaces, relieves residual stresses, enhances the microstructure of the part, and improves overall fatigue behavior [4, 28, 40, 46-48]. One such study by Qui et al. demonstrated the effect of HIP on porosity in AM Ti-6Al-4V samples. The authors observed that most pores closed, and the martensite was transformed into α and β phases after a HIP process [49]. Another study by Wycisk et al. investigated fatigue properties of AM Ti-6Al-4V after post-processing. The study

concluded that the HIP process effectively resolved defects inherent to the AM process, thus improving fatigue performance and reducing crack initiation [43].

1.3.2: Mechanical Surface Modifications

While the AM process is renowned for its ability to create parts with complex geometries, these intricate designs often prove challenging to mechanically polish. Mechanical polishing typically requires direct contact between the tool and the part which can be difficult when dealing with overhangs, channels, or lattice structures on AM parts. For this reason, obtaining a uniformly polished AM surface through traditional mechanical polishing techniques, such as machining and hand polishing, is very challenging [50-52]. Sandblasting is commonly used to modify an AM surface; however, this process still requires line of sight with the surface which is not always possible [53]. Residual stresses are known to form on surfaces that have been mechanically polished [4], with some studies noting that hardening can occur which may not always be desired [54, 55]. Consequently, alternative polishing methods that do not require direct contact with the workpiece have been explored.

1.3.3: Chemical Polishing

Chemical polishing in an alternative polishing technique that can be used for metallic AM parts. In this process, the workpiece is submerged in a corrosive solution, typically composed of harsh chemicals, such as hydrofluoric acid, and polishing is achieved without an external power supply. A viscous oxide film forms on the surface of the workpiece as it reacts with the corrosive solution. It is believed that peaks on the surface have a higher dissolution rate as the viscous oxide film is thinner at these points compared to the valleys. One of the advantages of chemical polishing is its ability to

access surfaces that are unreachable through traditional polishing techniques. However, the low polishing rates [56] and use of hazardous chemicals are significant deterrents to using chemical polishing [4].

1.3.4: Electropolishing

Another option when surface finishing metallic AM parts is electropolishing. This process utilizes an electric current to anodically dissolve the workpiece, resulting in a smoother surface free of impurities [57]. This process enhances corrosion resistance of AM parts by removing surface defects, such as oxides and non-metallic inclusions, and replacing them with a homogenous protective passive layer [51, 58]. Electropolishing also improves fatigue behavior through the removal of defects which can act as stress concentration sites [4]. One of the key advantages is that it requires no physical contact, allowing better access to hard-to-reach surfaces [51, 58] and avoiding the formation of residual stresses [4]. Additionally, part shape and dimension are less affected by the electropolishing process when compared to traditional polishing techniques [52, 59, 60]. Overall, it has been demonstrated that electropolishing is a viable option for polishing metallic AM parts [4, 57, 58, 61]. However, some disadvantages of electropolishing include the inability to remove deep scratches and non-metallic inclusions, and a heavy dependence on phase homogeneity. The following chapter discusses the electropolishing process in greater detail.

1.4: Fundamental Principles of Electropolishing

Electropolishing (EP) is a finishing process which modifies surface characteristics through the removal of material by electrolytic anodic dissolution. A standard electropolishing cell (Figure 2) is composed of an anode and cathode submerged in a conductive electrolyte. When a power supply is connected to both electrodes and an external potential is applied, the anode, otherwise known as the workpiece, is positively charged while the cathode is negatively charged. The anode oxidizes, losing electrons causing the metal ions to dissolve into the electrolyte. In contrast, the cathode gains electrons generating hydrogen through a reduction reaction on the cathode's surface in aqueous electrolytes [7]. Positively charged ions tend toward the cathode while negatively charges ions move away. The opposite movement of anions and cations generates an electric current [62]. The result of the anodic dissolution process is a modified surface that is often times smoother and brighter than the as-received part, along with a reduction in surface impurities [7].

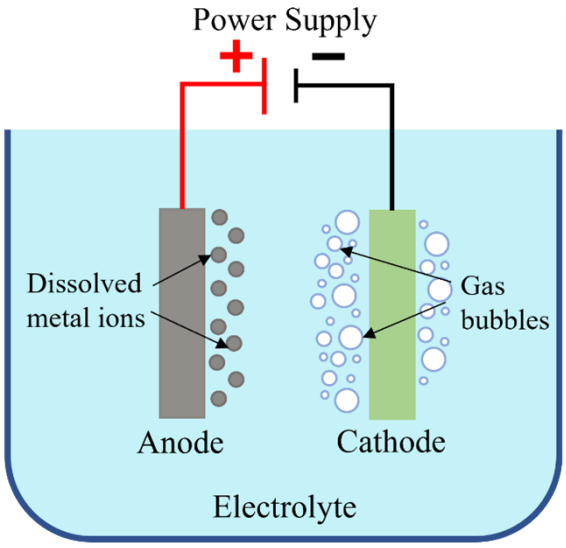

Figure 2. Schematic showing the electropolishing process (adapted from Han and Fang, 2019).

1.4.1: Defining Equations

During electropolishing, a current is applied to cause anodic dissolution of an anode's surface. In an acidic electrolyte, the primary reactions in the electropolishing of stainless steels includes the oxidation of iron (Equation 1), chromium (Equation 2), and nickel (Equation 3). These reactions can be represented as:

$$Fe \rightarrow Fe^{3+} + 3e^{-} \#(1)$$

$$Cr \rightarrow Cr^{3+} + 3e^{-} \#(2)$$

$$Ni \rightarrow Ni^{2+} + 2e^{-} \#(3)$$

$$2H_2O \rightarrow O_2 + 4H^{+} + 4e^{-} \#(4)$$

Hydrogen reduction on the cathodes surface can be described as:

$$2H_3O^{+} + 2e^{-} \rightarrow 2H_2O + H_2 \#(5)$$

As the metal ions dissolve into the electrolyte, the anodic surface becomes smoother.

1.4.2: Faraday's Laws

Electropolishing material removal rates generally follow Faraday's laws of electrolysis [63]. The first law relates the amount of material dissolved is proportional to the current passing through the system. The second law states that the amount of material dissolved by an equal quantity of electricity is directly proportional to their equivalent weights. These laws can be summarized by Equation 6 below,

$$m = \frac{MIt}{nF} \#(6)$$

where m is the amount of dissolved material in grams, n is the atomic valency, F is Faraday's constant, M is the atomic weight, I is the current in amps, and t is the polishing time in seconds. Equation 6 demonstrates that material mass removed, m, is dependent on the current I and total polishing time t [7].

1.4.3: Current Density-Voltage Curves

The kinetic behaviors of an electrochemical reaction are detailed in a current density-voltage (I-V) curve. The polarization curve is generated by gradually varying the voltage and plotting it against the current [7, 62, 63]. Figure 3 shows a characteristic I-V curve that is observed during the electropolishing process with four regions identified corresponding to etching, passivation, polishing, and gas evolution. In the etching region, current density increases linearly with voltage until reaching a maximum value and there is dissolution of the anode at the high energy sites (grain boundaries, etc). In the passivating region, a passive oxide layer is generated on the anodes surface which causes the current density to decrease slightly as the voltage increases and yield minimal material dissolution [7, 62]. The polishing regime exists as a limiting current plateau where the voltage continues to increase while the current remains relatively constant at a value where material dissolution is possible and occurs uniformly across the anode [7]. Here, the passivation is stabilized and anions from the anodes surface diffuse through the layer [62, 64, 65]. As the voltage continues to increase, the curve enters the gas evolution/pitting regime where the passive film breaks down. At this stage, oxygen begins to evolve on the anode and is easily trapped, causing pitting on the anodic surface. The I-V curve helps to guide parameter selection for electropolishing and ideally lands

somewhere in the polishing regime [7, 62].

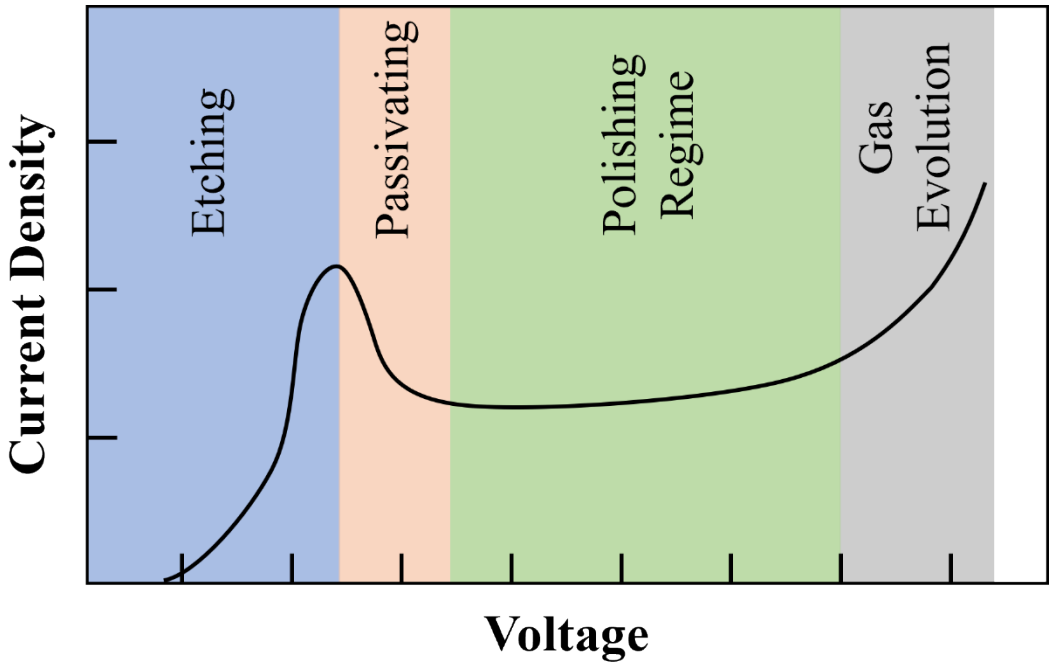

Figure 3. Current Density-Voltage curve (adapted from Han and Fang, 2019).

1.5: Fundamental Theories of Electropolishing

Electropolishing mechanisms are primarily driven by anodic dissolution and viscous films forming on the anodic surface. The driving mechanism is dependent on the anodic material and the electrolyte used. For example, in the electropolishing of stainless steel in an acid-based electrolyte, anodic dissolution may be favored as the iron and chromium are oxidized. The electrolyte and polishing material are critical factors in determining which electropolishing mechanism is favored [66].

1.5.1: Viscous Film Theory

The viscous film theory, initially proposed by Jacquet in 1935, has served as a foundation for electropolishing theories [67]. The theory suggests a film forms on the anodic surface during the electropolishing process because of dissolution products. The film is described to have a high electrical resistance which decreases current density and

limits material removal rates [62]. The viscous film is assumed to be flat on the side facing the electrolyte with an uneven thickness due to the peaks and valleys across the anode's surface. The thinner film at the peaks exhibits a lower electrical resistance allowing material to dissolve more rapidly compared to the valleys. The viscous film theory suggests that potential differences in material removal rates at the peaks and valleys of the anodic surface cause a polishing effect [7].

1.5.2: Mass Transport Theories

The salt film model, introduced by Grimm et al. [68], proposed a theory based on diffusion in which two salt films form on the surface of the anode due to an excess buildup of cations: a compact film and a porous film. The porous film is saturated with electrolyte containing anions and cations at the saturation concentration [7]. These ions conduct current through migration within the pores [62]. In the compact film, a solid dielectric barrier is formed, and cations are transported through solid-state ionic conduction in the presence of a high electric field. As the salt film thickens, the potential drop across the polishing region increases [7]. The diffusion of metal ions through the salt film is greater around the raised parts due to higher concentration gradients which regulates material removal rates and leads to smoothing. [62].

The adsorbate acceptor (AA) model was proposed by Matlosz et al. [69] and describes an alternative mass transport theory in the absence of a salt film. This theory suggests that metal cations dissolve and adhere to the anode's surface. For these cations to diffuse, they require an anion which reacts with the cation allowing it to diffuse away from the anodic surface. Mass transport is limited by the diffusion of the acceptor species

through the bulk electrolyte diffusion layer. Both the salt film and adsorbate acceptor models are used to describe electropolishing in current work.

1.6: Influence of Parameters

Electropolishing is heavily influenced by a variety of parameters which impact material removal rates and final surface finish quality. However, it is important to note that a universal electropolishing parameter set does not exist. Different materials, anode geometries, and electrolytes require a unique set of parameters which can be costly and time-consuming to define and optimize [4, 7, 62]. The following section will discuss the impact of electrolyte temperature, polishing duration, initial surface roughness, applied potential, and current signals on electropolishing results.

1.6.1: Electrolyte Bath Temperature

Electrolyte bath temperature is regarded as one of the most influential parameters in the electropolishing process, as it is directly related to mass transport [4, 7]. At higher bath temperatures, ion diffusion rates increase, facilitating the movement of ions away from the anodic surface [4] and the movement of acceptor ions towards the anodic surface [7]. Additionally, the solubility rate of ions in the electrolyte increases which contributes to an increase in the current density [4]. Elevated temperatures also reduce the viscosity of the electrolyte, providing fresh electrolyte to promote dissolution between the peaks and valleys of the surface [7]. An electropolishing study conducted on austenitic stainless steel in a solution of phosphoric and sulfuric acid tested bath temperatures of 60 °C, 70 °C, and 80 °C. The results corroborated the fact that current density values increased at the bath temperature increased (Figure 4) [70]. However, a study on

electropolishing aluminum samples in a solution of perchloric acid and ethanol yielded results that challenged this notion. Ma et al. concluded that high temperatures should be avoided, as a temperature of 40 °C would create pits on the aluminum surface [71]. Although elevated temperatures can increase the electropolishing effect, excessive temperatures can make it difficult to sustain a diffusion layer on the anodic surface, leading to unwanted etching or pitting due in part to excessive gas evolution [4, 7, 62].

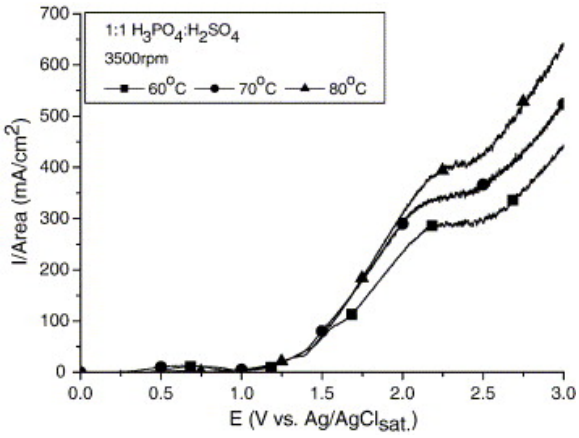

Figure 4. I-V curve of austenitic stainless steel in bath temperatures of 60 °C, 70 °C, and 80 °C.

1.6.2: Polishing Duration

Total polishing time is a critical factor that significantly influences the final quality of an electropolished surface. Electropolishing duration is dependent on initial surface roughness values. It is well established that surface roughness values experience a significant decrease during the early stages of electropolishing [4]. Wagner developed an equation to predict surface roughness changes during the electropolishing process as a function of several parameters, including polishing time [72]. Wagner predicted that as electropolishing time increased, the surface profile amplitude decreased exponentially – which was confirmed by several other studies [7, 64, 72, 73]. One such study was conducted by Lee, where it was observed that 316L stainless steel anodic surface

roughness decreased drastically at first then decreased slowly as polishing time increased [7, 64]. A study by Haidopoulos on the electropolishing of 316L stainless steel also found that surface roughness values decreased exponentially with time until reaching a limiting value [4, 7, 73]. Han and Fang claim that initial potential distributions between peaks and valleys are large, resulting in a quick polishing effect. However, as time passes and the surface becomes smoother, the potential differences decrease resulting in a slower polishing rate [7].

1.6.3: Initial Surface Roughness

As previously mentioned, final surface roughness values reach a limit and a major contributor is the initial surface roughness of the anode. [7]. Lee et al. conducted a study electropolishing nitinol samples in an acidic electrolyte, comparing results with initial surface roughness (R_a) values of 1 μm and 2 μm. After 50 s, the sample with the initial surface roughness value of 1 μm decreased to less than 0.5 μm; however, it did not decrease significantly with extended polishing time. After 300 s, the sample with initial surface roughness of 2 μm decreased to 0.98 μm with no significant improvements after 300 s (Figure 5) [1]. The results concluded that initial surface roughness values should be taken into account because of the natural limiting polishing effects during electropolishing [7].

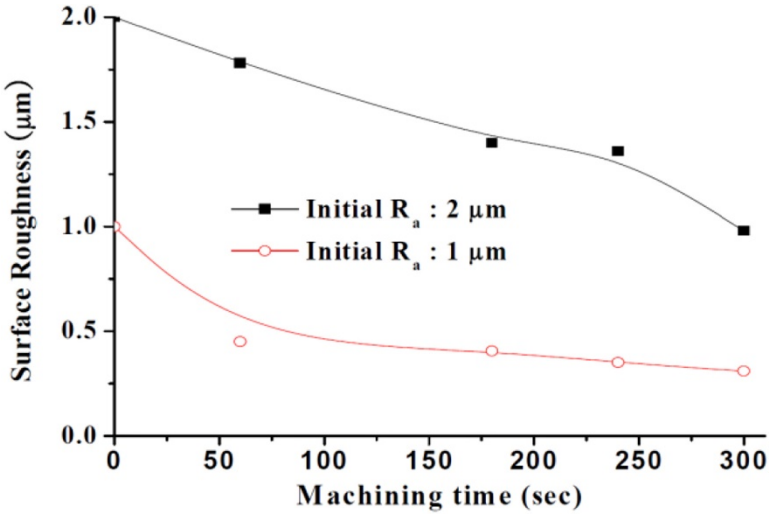

Figure 5. Plot of electropolishing time vs. initial surface roughness [1].

1.6.4: Applied Potential or Current

The applied potential is an important parameter as it directly influences the material removal rate in the electropolishing process. It is well understood that high voltages accelerate metal dissolution, however, excessive voltages may result in poor surface quality [4, 74]. Alrbaey et al. electropolished AM 316L stainless steel samples in a choline chloride ionic electrolyte with varying applied potentials between 4 V and 8 V. The results indicated that at higher voltages, there was non-uniform anodic dissolution which affected the dimensional accuracy of the part. The authors also found that potentials between 4 V and 5.5 V yielded the lowest surface roughness values [4, 74].

The overpotential electropolishing process is suggested for parts that have extreme surface roughness values, such as additively manufactured 316L stainless steels and maraging steels. The overpotential electropolishing process utilizes a voltage which is slightly above the voltage obtained from the polishing regime [4]. Chang et al. conducted a study using the overpotential electropolishing process for 20 min followed by a conventional electropolishing step for 20 min on additively manufactured 316L

stainless steel parts. The results indicated that the process was successful in removing cling-on powder particles while reducing the overall surface roughness values [3]. Determining an appropriate applied potential is vital to successfully dissolve material while avoiding unwanted damage to the anodic surface [4, 7].

1.6.5: Current Signals

Current signals influence material removal rates and resulting surface quality of the electropolishing process. It is well known that pulsed current waveforms, such as pulse/pulse reverse (PPR) currents and pulsed currents (PC), result in larger material removal rates when compared to direct currents (DC) [62, 75]. During the off-times of a PPR current, ion diffusion is facilitated, allowing for an even distribution of cations and anions within the electrolyte which is otherwise not found when using DC currents [62]. In addition, gas molecules diffuse off the surface resulting in less pitting. This can be attributed to the overall larger current density values experienced with pulsed currents [4, 7]. A study conducted by Ferchow et al. compared resulting Sa roughness values of electropolished additively manufactured 316L stainless steel internal pipe structures in a sulfuric and phosphoric acid-based electrolyte using DC, PPR, and PC. The results indicated that a brighter surface was observed with DC electropolishing, however, a smoother surface was obtained using PPR electropolishing.

1.6.6: Electrolyte Flow

Electrolyte flow is an important parameter in the electropolishing process as it influences mass transport and current distributions across the anodic surface. Electrolyte flow helps clear dissolved metal ions from the anodic surface. Datta and Landolt found that electrolyte flow helps to determine the overall electropolishing quality as current

distributions are influenced. The authors claimed that proper electrolyte flow promotes consistent material removal across the anodic surface as current density distributions are kept uniform [76].

1.7: Electropolishing Parameters Literature Review

Electropolishing is a delicate process which requires the adjustment of several parameters to create a uniformly polished part. While some parameters have been studied extensively, there are still several critical factors that are not yet thoroughly investigated. These include electrolyte composition, electrode gap, and cathode geometry which directly influence current density values on the anode's surface [4]. Uniform current density distributions on an anodes surface are vital in producing high-quality polished parts. The following section will go into detail on the current gaps in electropolishing literature pertaining to electrolyte composition, electrode spacing/gap, and cathode geometry.

1.7.1: Electrolyte Comparison

Electropolishing efficacy is highly dependent on the electrolyte composition used. Traditionally, metallic parts are electropolished with combinations of acids, such as sulfuric acid (H_2SO_4), phosphoric acid (H_3PO_4), perchloric acid ($HClO_4$), or hydrofluoric acid (HF) (Table 1) which are known to significantly reduce surface roughness values [4, 8-10, 12, 17, 51, 55, 77]. However, there are serious health and environmental risks that arise with the handling and disposing of such hazardous chemicals [5, 6, 78]. These aggressive electrolytes have also been shown to produce unwanted surface defects, such as pitting, in certain electropolishing conditions [4]. Due to this, some researchers have turned to alternative electrolytes composed of ethanol, ethylene, glycol or NaCl mixtures

[5, 6, 78]. These alternative electrolytes offer a more environmentally friendly option while reducing health hazards associated with traditional electrolytes. The following section will look at studies that were able to successfully use alternative electrolytes in an electropolishing process.

Table 1. Conventional electrolytes used to polish metallic AM parts (adapted from Chaghazardi, 2022).

AM Alloy	Electrolyte Chemical Composition	Voltage Range	Current Density Range
316L Stainless Steel	Phosphoric acid + sulfuric acid with/without water [9, 17, 51, 55]	$2\ V - 6\ V$	$500\ \frac{mA}{cm^2} - 800\ \frac{mA}{cm^2}$
Ti-6Al-4V	Perchloric acid + acetic acid with/without water[77] Hydrofluoric acid + acetic acid + sulfuric acid [4]	-	$160\ \frac{mA}{cm^2} - \ 320\ \frac{mA}{cm^2}$
CoCr	Phosphoric acid + sulfuric acid + water [79, 80]	$12\ V$	-
Inconel 625	Sulfuric acid + methanol [81]	$30\ V$	-
Inconel 718	Sulfuric acid + methanol [12]	$7\ V - 13\ V$	-

One study by Ferreri et al. developed a procedure to electropolish titanium (Ti) samples using a non-conventional electrolyte. Typically, Ti samples are electropolished in acidic electrolytes consisting of hydrofluoric, perchloric, and sulfuric acid [4]. Instead, Ferreri et al. utilized an ethanol-ethylene glycol-NaCl electrolyte to electropolish Ti samples. Their anodes consisted of pure α-Ti samples before and after plastic deformation, as well as alloyed Ti-6Al-4V samples created by additive manufacturing in both stress-relieved and heat-treated conditions. After electropolishing, the samples were then characterized using electron backscatter diffraction (EBSD). The results indicated that unpolished surfaces showed non-uniform areas of localized charge while the

electropolished surfaces showed a uniform charge distribution throughout. The authors successfully developed a procedure using a safer alternative electrolyte for electropolishing Ti samples [5].

Few studies have directly compared electropolishing results between conventional and alternative electrolytes. One of these studies was conducted by Han and Fang, where they compared NaCl-based electrolytes to conventional H_2SO_4-based electrolytes in the electropolishing of 316L stainless steel [6]. The alternative electrolyte they used was composed of a pure ethylene glycol solution containing NaCl with additional ethanol. The conventional electrolyte studied was a H_2SO_4-based electrolyte composed of 98 vol% sulfuric acid, 81 vol% phosphoric acid, and pure glycerol with a volume ratio of 5:4:1. They electropolished in a standard three-electrode cell utilizing an electrode gap of 10 mm. The electrodes consisted of a titanium mesh cathode and a flat 316L stainless steel anode. At room temperature, the NaCl-based electrolyte demonstrated overall lower surface roughness values (S_a) when compared to the traditional H_2SO_4-based electrolyte. At higher temperatures (66 °C), the Sa values were 20.4 nm and 100 nm for the NaCl-based electrolyte and H_2SO_4-based electrolyte, respectively. The results indicated that the environmentally friendly NaCl-based electrolyte outperformed the conventional H_2SO_4-based electrolyte in terms of reducing surface roughness [6].

Whether considering a conventional or alternative electrolyte, another important factor is the ionic mobility of species. Yang et al. suggests that environmentally friendly electrolytes, such as ethylene glycol, have reduced conductivity which may be beneficial in focusing the electric field on surface defects [62]. However, the low conductivity of environmentally friendly electrolytes presents other challenges. The reduced conductivity

and high viscosity can limit the mobility of ions within the electrolyte, leading to non-uniform current distributions and slower material removal rates across the anode's surface. Additionally, utilizing low-conductivity electrolytes may result in excessive heating which can lead to elevated gas evolution and pitting due to a higher electrolyte resistance, as noted in a study by Eozenou et al. [82]. Therefore, while alternative electrolytes offer certain advantages, their inherent properties may limit their effectiveness.

There is limited research comparing the effectiveness of conventional versus alternative electrolytes on AM metal surfaces, as of now. As previously discussed, AM parts possess heterogeneous microstructures that result in excessive surface roughness. The lack of extensive studies leaves a gap in understanding how different electrolytes can address the specific challenges unique to AM surfaces. Further investigation is needed to evaluate the performance of alternative electrolytes on AM metal surfaces.

1.7.2: Electrode Spacing

To date, there are few studies investigating the effect of varying electrode gap on electropolishing, especially within the realm of additive manufacturing [4]. There are even fewer studies examining the effect of particularly small electrode gaps (~less than 5 cm). The limited number of studies on this topic is surprising, given the widely acknowledged effect of electrode gap on current density [78]. As the electrode gap decreases, there is a lower ohmic voltage drop and the current density typically increases, resulting in reduced surface roughness values [11, 64].

One study by Lassel investigated the impact of varying electrode gap in final surface roughness values of electropolished surfaces. Lassel electropolished additively

manufactured Ti_6Al_4V samples in a non-aqueous, alcohol-based electrolyte composed of 70 vol% ethyl alcohol and 30 vol% isopropyl alcohol. Electrode spacing was varied from 5, 7.5, and 10 mm and polishing time from 60, 300, 600, and 1200 s. After electropolishing for 60 s, the surface roughness (Ra) values were ~20, 22, and 23 μm for the electrode gaps of 5, 7.5, and 10 mm, respectively. After the samples were polished for 1200 s, the roughness values dropped to ~7.5, 15, and 20 μm, respectively. Overall, a trend emerged indicating that the smaller electrode gap resulted in lower surface roughness (Ra) when compared to larger gaps of equal polishing time [8].

Another experiment conducted by Chaghazardi looked at the effect of electrode gap on electropolishing results, specifically focusing on final surface roughness and surface brightness. Chaghazardi electropolished 316 stainless steel tubes (outer diameter of 25.5 mm) with cathode tubes of varying diameters (2, 8, 12, and 15 mm) placed within the anode. The tube was electropolished at a potential difference of 4V for 20 minutes in an electrolyte of 50 vol% phosphoric acid, 35 vol% sulfuric acid, and 15 vol% water. The results indicated that the final surface roughness varied only slightly with changes in the electrode gap. However, a major difference was observed between the surface brightness of each sample. The smallest electrode gap produced a significantly brighter surface compared to the larger gaps upon visual inspection [9]. Lassel and Chaghazardi both concluded that the smallest electrode gap tested produced the best results in terms of either surface roughness or brightness [8, 9].

However, achieving the smallest possible electrode gap may not always be the most desirable because it can result in the formation of pits and bubble marks on the anodes surface. Han and Fang electropolished a 1 mm diameter tungsten wire mounted in resin

with a flat copper sheet in a NaOH electrolyte of different concentrations. They tested different electrode gaps which varied from 0.15, 0.5, 1, and 1.5 mm. The authors demonstrated that the surface finish improved as the electrode gap was reduced; however, if the gap were too small (0.15 mm) it could lead to the formation of pits on the surface. Han and Fang found that the ideal electrode gap was 0.5 mm because it resulted in an optimal current density while avoiding bubble effects on the surface [78]. Notably, their idealized electrode gap is considerably smaller than those reported in most other studies [8, 9].

1.7.3: Custom Cathodes

Although additive manufacturing can create increasingly complex structures, a significant challenge emerges in the electropolishing of these intricate designs. Several studies have demonstrated the struggle to attain uniform polishing on both internal and external surfaces of an AM structure [4, 9, 51]. The underlying cause of this issue has been attributed to non-uniform primary current distributions over the complex additively manufactured components [66, 83-85]. The local current density of an additively manufactured part is dependent on cell geometry, shape, and part position if mass transport and charge transfer are neglected. The complex details on an AM surface may be physically unreachable by a cathode which can influence a non-uniform polishing effect [4].

To date, there are few studies investigating the impact of cathode geometry on electropolishing results, as most of the research employs flat or cylindrical cathode geometries [6, 8-11, 78]. The following section describes some of the few studies outlining the implementation of a customized cathode.

In a study conducted by Urlea and Brailovski, an electropolishing setup was designed to simulate the polishing of an internal surface of a tube through careful arrangement of the electrodes. The study primarily aimed to investigate the effects of additive manufacturing build direction on electropolishing behavior, however, it also touched on the effects of cathode conformity and proximity. The electropolishing experiment was conducted with AM Ti-6Al-4V electrodes in a 60 vol% perchloric acid and glacial acetic acid in a 1:9 volume ratio. The anodes were printed in a stave geometry with different build angles and placed in a circular arrangement with other anodes. The cathode consisted of a star-shaped geometry placed in the center of the anode arrangement. The results showed that the surface roughness (R_a) value was improved as much as 92% and build orientation has little effect on the amount of material dissolved [77].

Lynch et al. conducted a study investigating the effects of a conformal cathode tool on electropolishing deep into a lattice anode structure. The electrodes used for this study were additively manufactured with Inconel 718. The anode was a cubic lattice structure composed of unit cells with an overall dimension of 4 mm. The cathode assembly was built to surround the exterior of the anode cube while also being inserted between the lattice anode structure. The authors used a potential difference of 7V, and a current of 13A to electropolish the lattice structures for 30 minutes. The electrolyte composition was: ethanediol, ammonium nitrate, ammonium chloride, ammonium sulfamate, and water. Surface roughness values of the internal lattice anode were measured to be reduced on the order of 70%. Results showed a significant amount of material was removed deep into the lattice structure. COMSOL modeling results verified their experimental results

by demonstrating that material removal rates are lower on surfaces further from the cathode, highlighting the importance of cathode conformity and proximity [12].

1.8: Research Objective

The purpose of this study was to investigate the effects of cathode geometry, electrode gap, and electrolyte composition on the electropolishing of LPBF 316L stainless steel. Additionally, a COMSOL model was developed to inform cathode design. The specific goals of this research were:

1. Determine the effect of increasing cathode conformity on surface roughness, reflectivity, mass, and profilometry.
2. Determine the effect of varying electrode spacing on surface roughness, reflectivity, mass, and profilometry.
3. Compare electropolishing results between a traditional acid electrolyte and an alternative, environmentally friendly NaCl-PEG electrolyte.
4. Develop a COMSOL model to inform cathode design and create a unique cathode that ensures uniform current density distributions across an anode's surface.

Chapter 2 – Experimental Methods

2.1: Sample Preparation

LPBF anodes and cathodes were printed on 3D Systems ProX-200 using 316L stainless steel powder provided by (3D Systems). A total of 28 T-shaped anodes were printed on a single 316L build plate. The print parameters for all samples are summarized in Table 2. The general chemical composition of the LPBF powder can be found in Table 3. The T-shaped samples were printed normal to the build plate, as shown in Figure 6a-b, to guarantee that the initial roughness of all tested surfaces was consistent. Figure 6b-c also shows a schematic of a T-shaped sample with labeled surface orientations top, bottom, front, left, left-wall, and back. Parts were removed from the build plate using wire electrical discharge machining (EDM) with a brass wire.

Table 2. LPBF sample printing parameters.

Machine Model	Power (W)	Scanning velocity (mm/s)	VED (J/mm^3)	Hatch spacing (µm)	Layer thickness (µm)	Scan Pattern
3D Systems ProX200	113	1400	54	50	30	Hexagon

Table 3. Printing powder chemistry.

Wt%	Al	C	Cr	Cu	Fe	Mn	Mo	N	Ni	O	S	Si
	0.003	0.018	17.12	0.15	67.2	1.28	2.19	0.12	11.18	0.11	0.013	0.49

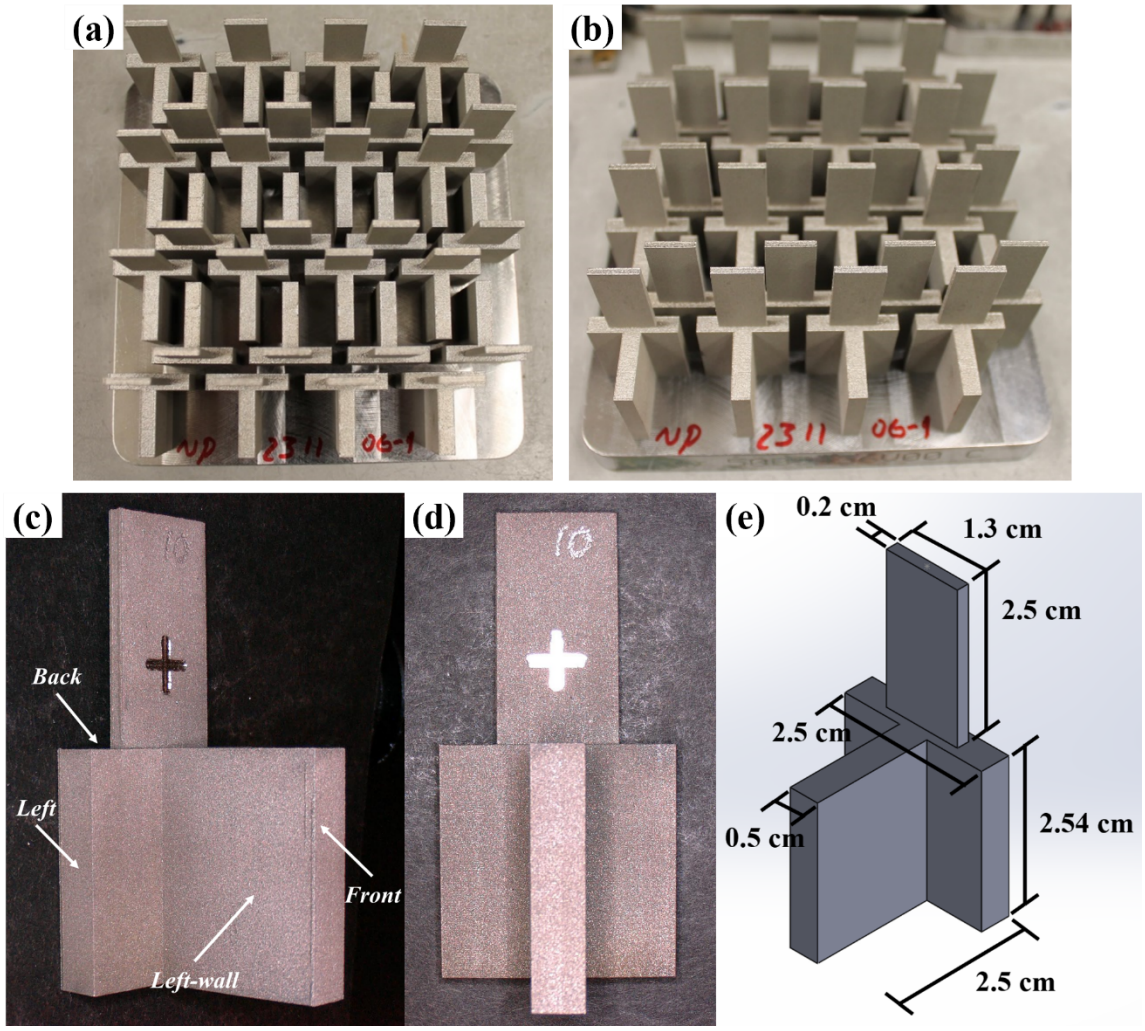

Figure 6. (a-b) Images of T-shaped anodes on their build plate, (c-d) images of a labeled T-shape, and (e) schematic of a T-shape including dimensions.

Cathodes were printed according to 3 different latticed geometries, flat, cylindrical, and conformal. Each cathode geometry was printed on its own individual build plate. The flat lattice cathode was printed in a direction parallel to the build plate as shown in Figure 7a. The cylindrical and conformal lattice cathode geometries were printed in a direction normal to the build plate, as shown in Figure 7b-c. To test the effect of electrode spacing on electropolishing efficacy, varying sizes of cylindrical and conformal lattice cathodes were created- although, for the purposes of this study, only the two smallest sizes per cathode were tested. The two sizes used for the cylindrical lattice

cathodes were of diameters 3.5 cm and 9.5 cm. The sizes used for the conformal lattice cathodes created electrode spacings of 2 mm and 20 mm.

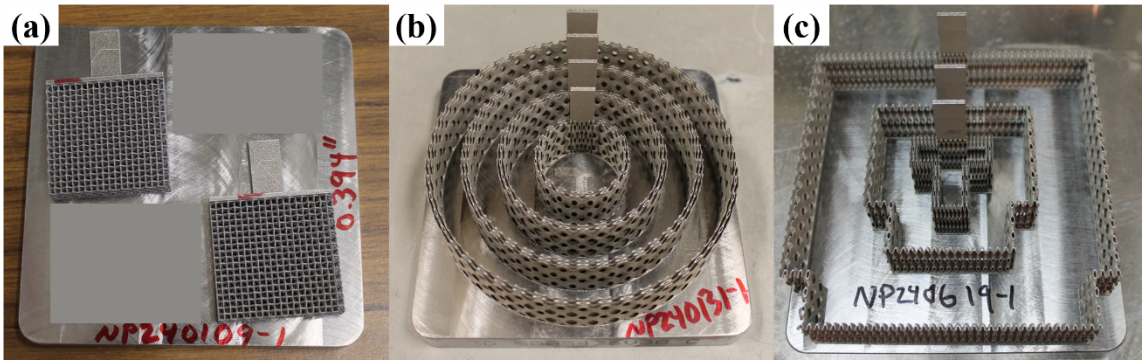

Figure 7. Build plate images of (a) flat cathode, (b) cylindrical cathode, and (c) conformal cathode.

After the T-shaped anodes were removed from the build plate, fiducial markings, as shown in Figure 8, were engraved on their tabs using a drill press. This fiducial marking served as a reference point to align images taken before and after polishing.

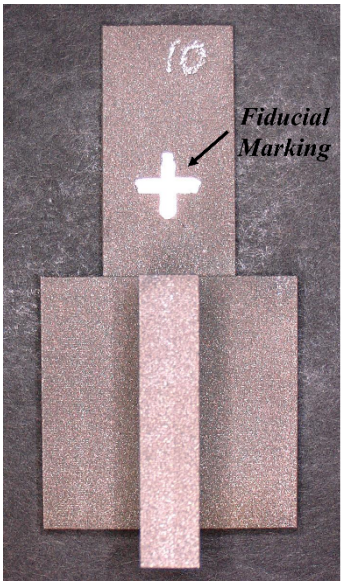

Figure 8. Image of a fiducial marking on a T-shaped part.

Prior to electropolishing, the as-printed T-shaped anodes were sonicated for 10 min in ultrapure Millipore water (18.2 MΩ cm) deionized (DI) water followed by a 10

min sonication in acetone. Samples were then dried with house nitrogen gas. The as-printed cathodes were submerged in a 10 vol% nitric acid bath for 10 min. The cathodes were then rinsed with DI water and dried with house nitrogen gas. The nitric bath cleaning process was repeated for both the anode and cathode after electropolishing to remove contaminants.

Each anode had a total exposed surface area of approximately 25 cm^2 which included the front, left-wall, left, back, right-wall, and right orientations (Figure 6c). Top and bottom surfaces of the T-shaped anode were masked-off to limit the amount of surface area exposed to the electrolyte. Anodes were masked using a liquid epoxy (3M™, Scotchkote™ Liquid Epoxy Coating 323, USA).

2.2: Surface Characterization

2.2.1: Mass Measurements

After undergoing the cleaning process, T-shaped anodes were placed in a desiccator (Fisherbrand™, Massachusetts USA) overnight to remove excess moisture. Mass measurements of the anodes were then collected using an analytical balance (Mettler Toledo, XP105 Semi-Mirco Analytical Balance, USA) and recorded for both the as-printed and polished state.

2.2.2: Reflectance Measurements

Reflectance measurements were obtained in the center of the back surface of the T-shaped anodes (Figure 9a) to standardize the imaging area. Measurements were made with a DH-2000 Deuterium-Halogen Light Source that covers a range of 200-2500 nm, the Ocean QE Pro High Performance Spectrometer UV-VIS-NIR, and an ISP-R Fiber Optic Integrating Sphere of 30 mm diameter with a spectral range of 200-2500 nm

(Ocean Optics, USA) (Figure 9b). Connections were established between the light source, integrating sphere, and spectrometer with fiber optic cables. The Deuterium-Halogen Light Source was allowed 20 min to warm up before acquiring any measurements. A reflectance standard was used as a reference according to standard WS-1-SL. Specular measurements were acquired by capturing the reflection of light at 90 degrees. Further acquisition parameters are shown in Table 4.

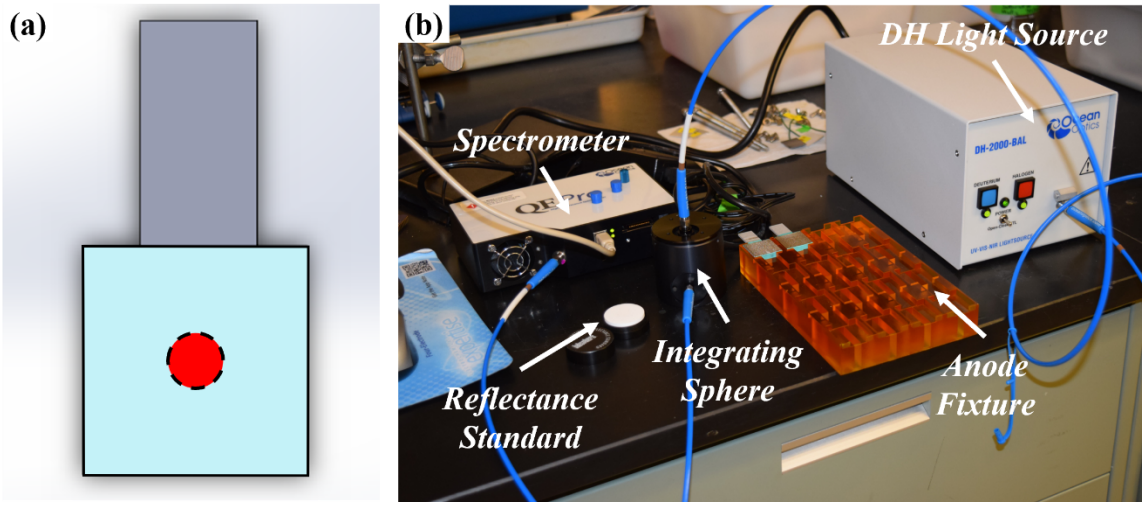

Figure 9. (a) Schematic of T-shape back surface with reflectance measurement area outlined, and (b) image of reflectance measurement setup.

Table 4. Additional parameters for reflectance measurements.			
Integration Time	**Scans to Average**	**Boxcar Averaging**	**Non-linearity Correction**
Automatic	1	5	On

2.2.3: Topographical Measurements

Surface topography of each sample was measured using two different instruments utilizing non-contact, optical-based techniques. Optical surface roughness measurements of 4 orientations on the T-shaped anode (front, left, left-wall, and back) were obtained using white light interferometry (Zygo, NexView, USA). An area of 2.8 x 2.8 mm was

scanned and stitched together from the center of each surface with a 3 x 3 Gaussian denoising filter (no other filters were used). Using the metrology software (MountainsMap® V 7.4), roughness values, including average surface roughness (S_a) and maximum surface peak/depth (S_z) were extracted from a 2.5 x 2.5 mm area, according to ISO 25178. Measurements obtained through white light interferometry were corrected for general tilt. Topographical measurements were performed on the anodes cleaned surfaces (Figure 10) in the as-printed and polished state.

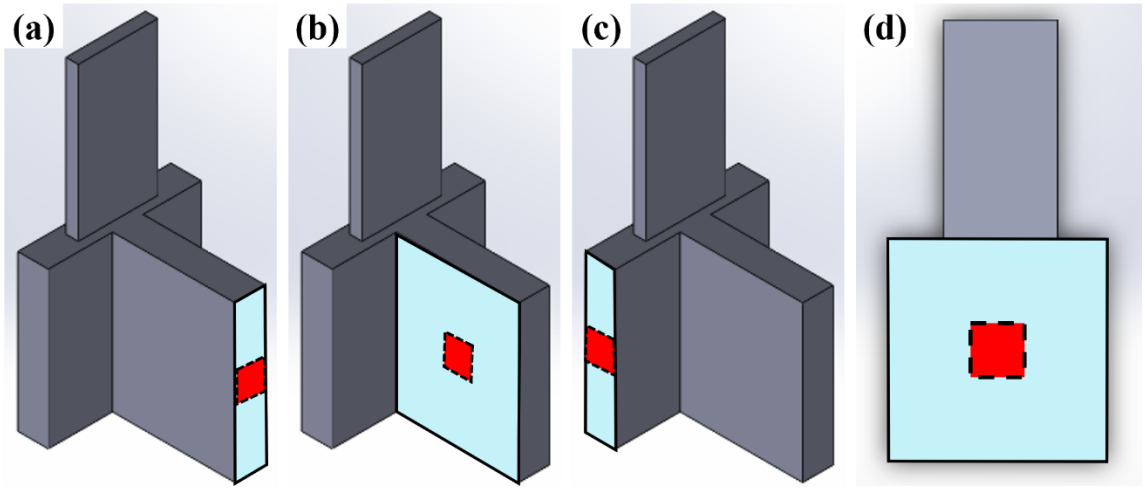

Figure 10. Schematics detailing the standardized area for capturing optical images on the: (a) front face, (b) left-wall, (c) left side, and (d) back surface.

2.2.4: 3D Optical Profiler

The Keyence VR-6000 uses while light triangulation and a motorized rotation unit to optically profile surfaces in the 3D space. This instrument projects a white light pattern which is distorted and correlated to height. The samples were rotated and imaged in 360° and resulting images were stitched together to create a 3D scan of the entire sample. Images were captured using a low, 12x magnification. The z resolution is listed by the manufacturer as 400 nm. 3D optical scans were obtained using the same model of machine at two distinct locations (Los Alamos and Albuquerque, New Mexico).

2.2.5: Optical Imaging

Macroscopic optical images were captured on a microscope using a 5x magnification (Keyence, VHX5000, USA). The samples were imaged with this magnification in a 45° and top-down view, as shown in Figure 11.

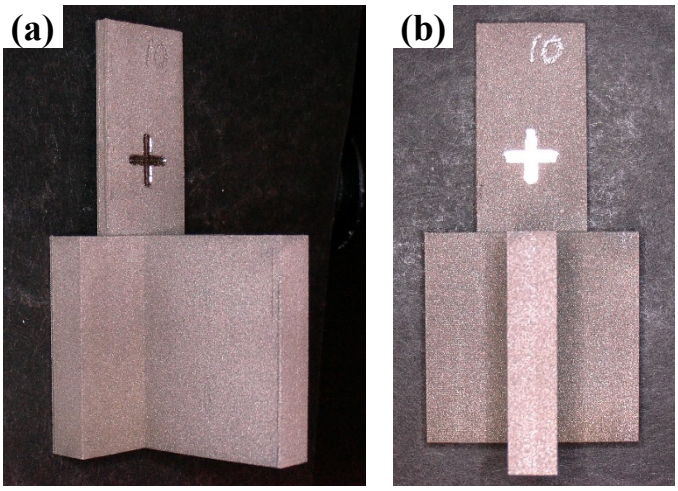

Figure 11. (a) T-shape imaged at a 45° view. (b) T-shape imaged in a top-down view.

Microscopic optical images were acquired with a microscope at two different magnifications: 20x and 200x (Keyence, VHX 7000, USA). The imaging area was standardized by acquiring images in in the center of each surface as shown in Figure 10. All samples were imaged in the as-printed and polished states.

2.3: Electrolyte Composition

This study compared two electrolytes of different compositions: an environmentally friendly electrolyte and a conventional acid electrolyte. Each electropolishing test was performed in a 1,600 mL bath of the respective electrolyte.

The environmentally friendly electrolyte consisted of a NaCl-polyethylene glycol (PEG) solution of 36 vol% 6M NaCl and 64 vol% polyethylene glycol. The electrolyte was prepared using the following procedure: a 6M NaCl solution was created by slowly dissolving 201.92 g NaCl in 576 mL DI H_2O using a magnetic stir plate. The NaCl

solution was then combined with 1,024 mL of PEG, diluting the solution to a 2 M NaCl solution. Mixing this electrolyte triggers an exothermic reaction, therefore, it was allowed to cool 1 hour before use. A new batch of NaCl-PEG electrolyte was produced for each electropolishing test.

The conventional acid electrolyte consisted of 50 vol% phosphoric acid, 25 vol% sulfuric acid, and 25 vol% glycerol added to extend the bath life. The electrolyte was prepared by first combining 800mL phosphoric acid with 400 mL sulfuric acid and placing the solution in a water bath to cool while stirring with a magnetic stir plate for 1 hour. Then, 400 mL of glycerol were added to the solution and stirred vigorously to combine. The acid electrolyte bath was discarded after polishing 3 samples.

Immediately before electropolishing, the conductivity of the electrolyte was tested using a calibrated conductivity probe (Traceable™, Conductivity Meter, USA). The conductivity range of the probe is 0.1-199.9 μS with an accuracy of ±0.3% + 1 digit.

2.4: Linear Sweep Voltammetry (LSV) Scans

Prior to running electropolishing tests, electrochemical measurements were conducted on wrought stainless steel, flat coupons using a standard three electrode cell with a stainless steel mesh counter electrode and a Ag/AgCl (saturated KCl) reference electrode (+0.197 V vs. SHE). The flat coupons (dimension x dimension x dimension) were masked using a liquid epoxy (3M™, Scotchkote™ Liquid Epoxy Coating 323, USA) to control the amount of area exposed. The exposed area values were either 1 cm^2, 2 cm^2, or 4cm^2.

Anodic potentiodynamic polarization measurements were carried out to determine each samples polishing window (Figure 3) on a Biologic VMP300 multichannel

potentio/galvanostat. The samples were immersed at open circuit potential (OCP) for 10 min in the environmentally friendly NaCl-PEG and acid-based electrolyte. The potentiodynamic measurements started 0.5 V below the samples OCP and scanned at rates of either 0.5, 1, 3, 5, or 10 mV/s in the anodic direction to +1.5 $V_{Ag/AgCl}$ or the experiment was stopped when a current density of ~100 mA/cm^2 was reached.

2.5: Electropolishing

Prior to electropolishing, an stainless steel wire was attached to the tabs of the smallest cylindrical and conformal cathodes, as seen in Figure 12, with tack welds. This facilitated the connection to the power supply. Both anode and cathode were submerged in a 10 vol% nitric acid bath for 10 min to remove any contaminants prior to electropolishing.

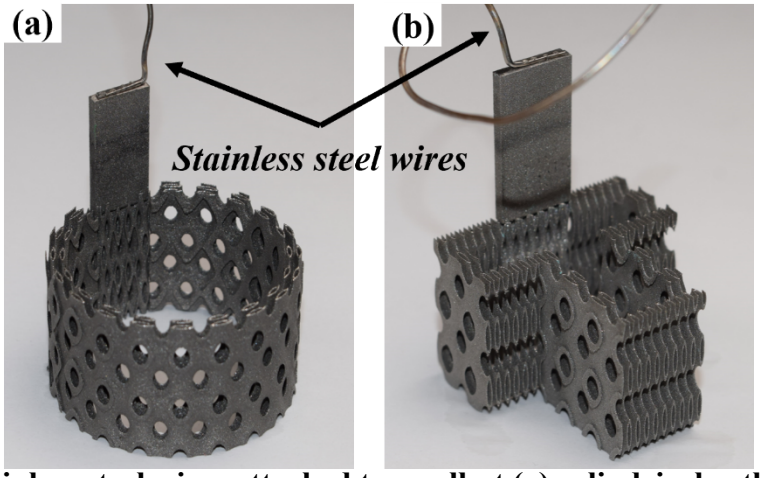

Figure 12. Stainless steel wires attached to smallest (a) cylindrical cathode, and (b) conformal cathode.

A copper braid was used to establish a connection between the terminals of the power supply (Dynatronix, Microstar DP/DPR Model, USA) and the threaded electrode holders. A current probe (BK Precision, CP62 Current Probe, USA) was attached to the copper braid connected to the negative terminal of the power supply. The current probe readings

were recorded using a data acquisition system (DATAQ, DI-245 Thermocouple and Voltage Data Acquisition System, USA) every 20 ms. The electropolishing bath containing a stir bar was placed over a magnetic stir plate which was set to 300 rpm intended to help with agitation and flow. The electrode holders were carefully placed to fully submerge the electrodes in the electrolyte while keeping their respective tabs above the water line. The electrode spacing between anode and cathode was controlled with a polycarbonate 3D printed fixture individualized to maintain a uniform spacing for each cathode geometry (flat, cylindrical, conformal, and selective). An image depicting the electropolishing experimental setup can be seen in Figure 13.

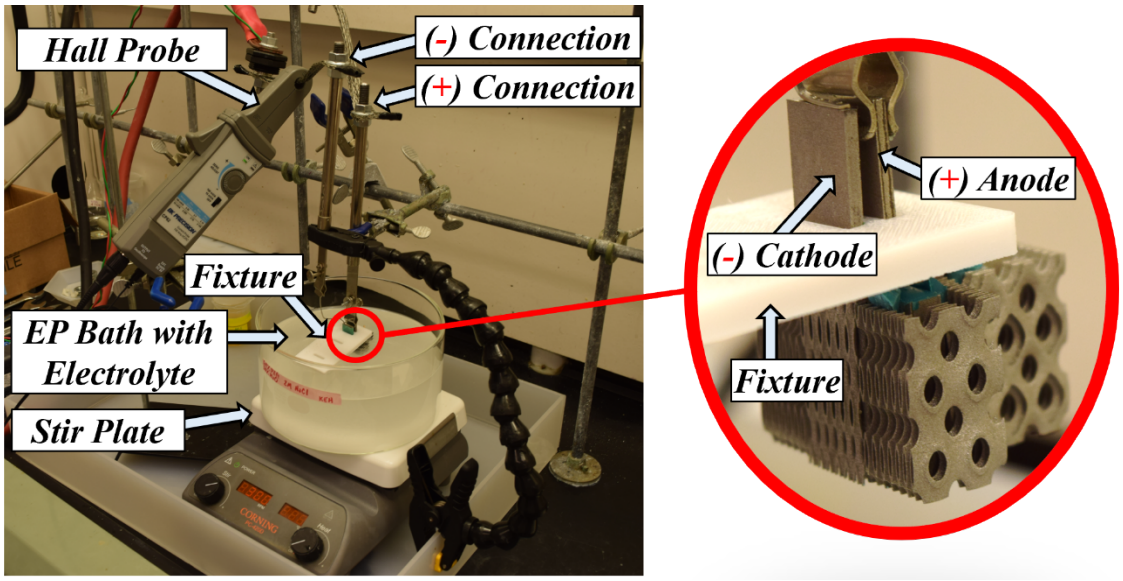

Figure 13. Image of a labeled electropolishing experimental setup.

For this study, two different electrode spacings were tested per cathode geometry: 2 mm, and 20 mm. Figure 14 demonstrates how the anode and cathode were placed relative to one another for each cathode geometry at the smallest spacing.

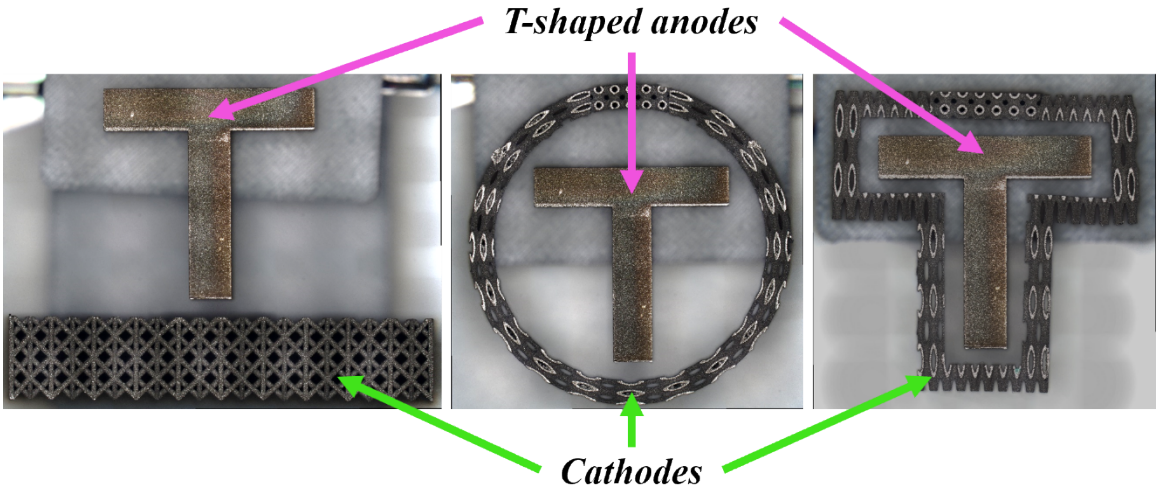

Figure 14. Images demonstrating the closest electrode spacing for different cathode geometries.

The electropolishing took place over 40 min in both electrolytes. A current density of ~80 mA/cm^2 (total applied current of 2 A) was used in the NaCl-PEG electrolyte and ~560 mA/cm^2 (total applied current of 14 A) was used for the acid electrolyte based on results from the polarization scans (adjusted for rough AM surfaces). A pulse of 25 ms on and 25 ms off was used to allow for diffusion, especially in an electrolyte as viscous as NaCl-PEG. Table 5 summarizes and compares electropolishing parameters between the two electrolytes.

Table 5. Electropolishing parameters for both electrolytes.		
Parameters	**NaCl-PEG Electrolyte**	**Acid Electrolyte**
Current	2 A	14 A
Current Density	~80 mA/cm^2	~560 mA/cm^2
Exposed Area	25 cm^2	25 cm^2
Masking Technique	Skotchkote™ Epoxy	
Pulse	25 ms **ON** / 25 ms **OFF**	
Total Polishing Time	40 min (20 min effective polishing time)	
Flow	Stir bar @ 300 RPM	

Chapter 3 – Computational Methods

3.1: Introduction

COMSOL Multiphysics was utilized to guide the development of a "selective cathode" which was created to achieve uniform current distributions on the anode's surface. The objective of the selective cathode was to prevent targeted electropolishing at the exterior corners of the anode while still effectively targeting the inner corners, thereby creating a more uniform electropolishing effect across the entire surface. The COMSOL model was constructed using primary current distribution and deformed geometry interfaces to simulate the electropolishing process. The model allowed for the evaluation of local current density values at various points on the anode's (and cathode') surface. The selective cathode was designed to minimize the range of current densities to ensure a uniform electropolishing result.

3.2: Model Physics

Utilizing COMSOL multi-physics, a fully coupled 2D model was created to study current density distributions across the T-shaped anode's surface using a variety of cathode shapes and electrolyte conductivities. The deformed geometry, primary current distribution interface, and Multiphysics interface were used along with a time-dependent study. The primary current distribution interface describes both the transport of ions in an electrolyte, which is assumed to have a uniform composition, and current conduction in electrodes using a charge balance and Ohm's law. Activation overpotentials resulting from charge transfer reactions are neglected. This interface allows for the estimation of ohmic loses in electrochemical cells that have been simplified. The domain equations for the primary current distribution are derived from the Nernst-Planck equations which

describe the flux of charged species through diffusion, migration, and convection. However, it is important to note that in the primary current distribution interface, convection and diffusion terms are neglected, making it solely dependent on migration (i.e. electrolyte conductivity) [86]. The current density vector in an electrolyte using the primary current distribution interface is as follows:

$$i_l = -F^2 \sum z_i^2 u_{m,i} c_i \nabla \varphi_l \#(7)$$

Where i_l is the current density vector in an electrolyte, F is the Faraday constant, c_i is the concentration of the ion, z_i is the valency of the ion, $u_{m,i}$ is the mobility of the ion, and φ_l is the electrolyte potential. The conductivity of the electrolyte, assuming a uniform composition, can then be expressed by:

$$\sigma_l = F^2 \sum z_i^2 u_{m,i} c_i \#(8)$$

Thus, the current density in the electrolyte can be rewritten by:

$$i_l = -\sigma_l \nabla \varphi_l \#(9)$$

Indicating that the current density value is dependent on the product of electrolyte conductivity and electrolyte potential [86].

3.3: Model Setup

3.3.1: Geometry

The geometry of the 2D model was constructed to represent the physical 3D electropolishing system. The T-shape anode was modeled with rectangular elements, reflecting the actual dimensions of the part (Figure 6e). Initially, three iterations of the model were designed with varying cathode geometries representing the flat, cylindrical, or conformal cathode geometry. The electrode spacing was varied according to experimental measurements. Figure 15 shows a schematic of the three cathode

geometries at the closest spacing of 0.2 cm.

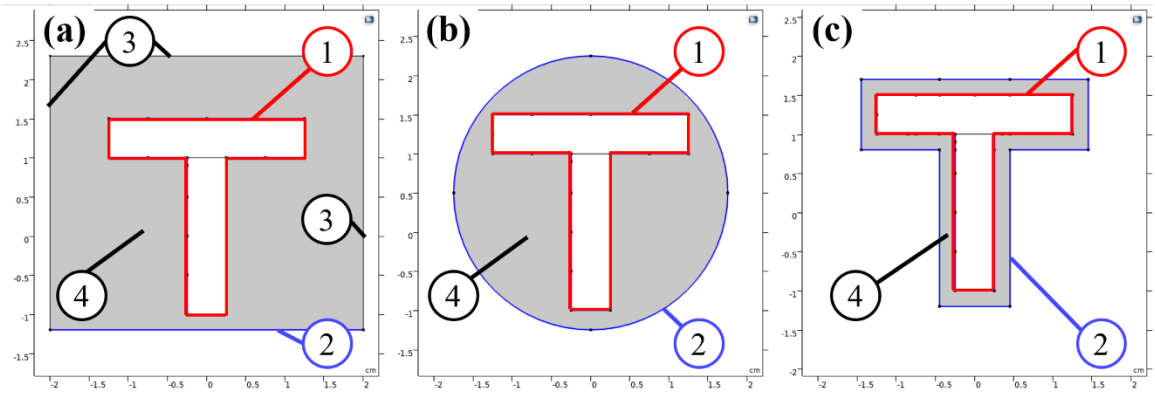

Figure 15. Schematic of model geometry and boundary conditions for (a) flat cathode, (b) cylindrical cathode, and (c) conformal cathode.

3.3.2: Model Parameters

The electrical conductivity of the electrolyte and average current density were set to 1 S/m and 80 mA/cm^2, respectively, based on experimental measurements obtained using the environmentally friendly NaCl-PEG electrolyte. The dissolving species was assumed to be iron (Fe), and its density (7850 kg/m^3) and molar mass (0.05584 kg/mol) values were obtained from literature sources [36].

3.3.3: Boundary Conditions

The boundary conditions of the primary current distribution interface are illustrated in Figure 15. The anode and cathode surfaces (boundary 1 and 2, respectively, as shown in Figure 15) both act as electrode surfaces within the model. The anode surface on boundary 1 is designated as the electric ground, with a potential of 0 V. The cathode surface on boundary 2 is set to apply an average current density of 80 mA/cm^2. The electrolyte domain on boundary 4 is assigned an electrical conductivity of 1 S/m. Additionally, the Multiphysics interface is incorporated to control deformation boundaries. The boundary conditions are summarized in Table 6.

Table 6. Summary of Boundary Conditions		
	Boundary	**Definition**
Boundary	1	Anode / Electric Ground
	2	Cathode / Current Density
	3	Insulation
Domain	4	Electrolyte Conductivity
	4	Electrolyte Insulation
Multiphysics	1	Deformation
	2,3	No Deformation

3.3.4: Mesh

The automatic mesh creator module and corner refinement interface were utilized to generate a triangular mesh. The predefined mesh size was set to “fine” with a maximum and minimum element size of 0.186 cm and 0.00105 cm, respectively. The minimum angle between boundaries utilized for the corner refinement interface was set to 240° with an element size scaling factor of 0.25. Figure 16 depicts the mesh with added corner refinement for the three cathode designs.

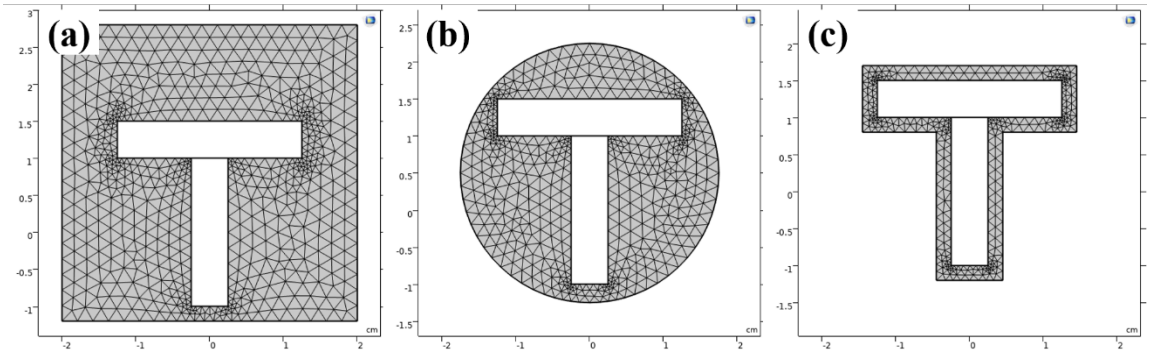

Figure 16. Schematics of meshes used to model the (a) flat cathode, (b) cylindrical cathode, and (c) conformal cathode.

3.4: Selective Cathode Design

The selective cathode design process began with a point evaluation in the COMSOL model. In COMSOL, the point evaluation involves calculating a specific variable at a single point within the model. For this study, the variable of interest was the local current density value at the points indicated in Figure 17. The objective was to design a cathode that would minimize the range of local current density values across all points, thereby achieving the most uniform current density distribution across the surface among the tested cathodes.

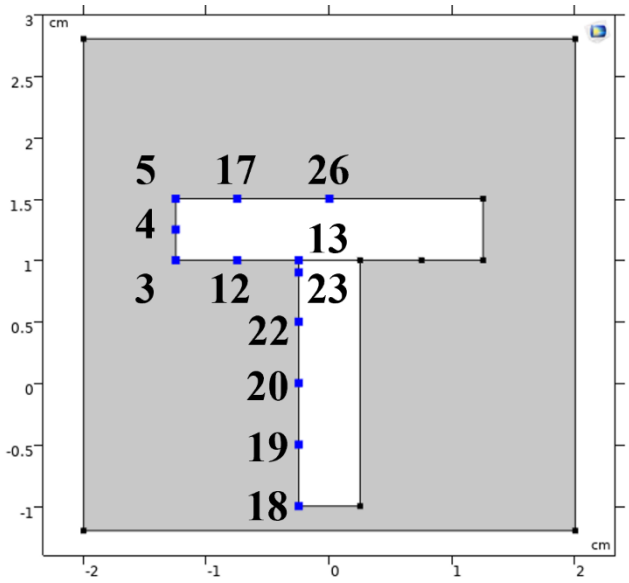

Figure 17. Labeled schematic of COMSOL point evaluations.

The point evaluation analysis began with the flat, cylindrical, and conformal cathode geometries (Figure 15). The T-shaped anode was assumed to be symmetric. The results from the analysis indicated that the local current density at the exterior corners (generally points 5, 3, and 18) was significantly higher than the values at the interior corners (point 13). To mitigate this, the cathode geometry was modified by extending it into circles at the exterior corners, as shown in Figure 18a. However, the flat edges of the

cathode exhibited low current density values, requiring further modifications to the cathode geometry as illustrated in Figure 18b-c. This configuration essentially represents the conformal cathodes with circles/semicircles at the exterior corners. To increase the distance between the anode and cathode at the corners, a circle was added to each exterior corner, as shown in Figure 18d. The positions and dimensions of the circles were modified as shown in Figure 18e-g. Finally, an elliptical cathode was tested, as seen in Figure 18h. The cathode geometry shown in Figure 18e resulted in the lowest range of local current density values among the selected points and was therefore chosen was the optimal selective cathode geometry.

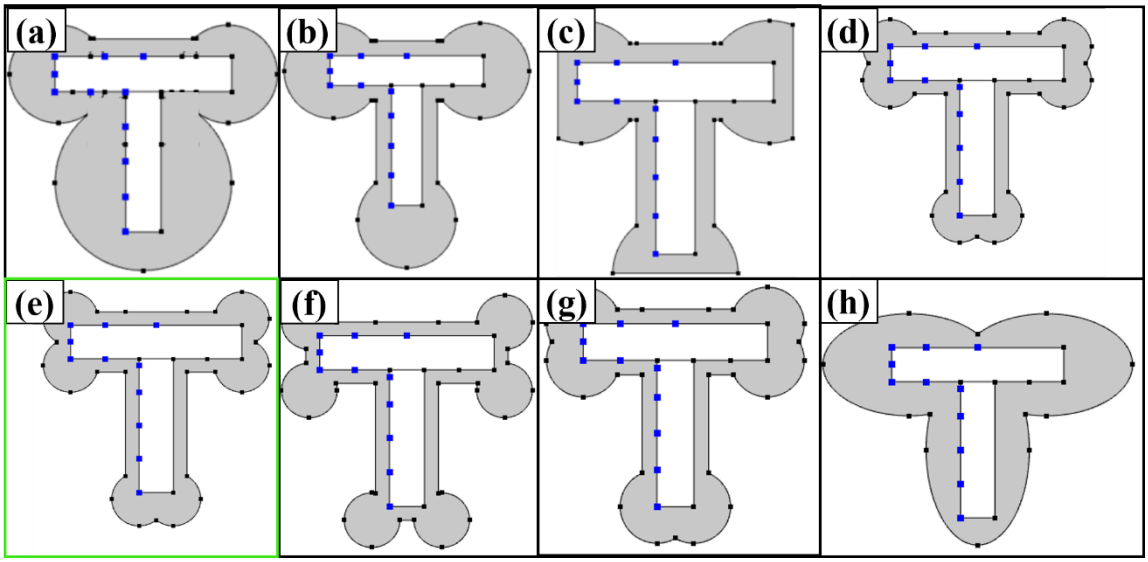

Figure 18. Schematics of iterations for the selective cathode design.

3.4.1: Selective Cathode

The selective cathode was printed with similar powder chemistry and the same print parameters and techniques as described for the other cathodes in the preceding experimental section. The cathode was printed in a direction normal to the build plate, as illustrated in Figure 19a. The selective cathode and its dimensions are shown in Figure

19b-c. Lesson's learned from printing the conformal cathode led to thickening the lattice structure to improve the rigidity of the selective cathode.

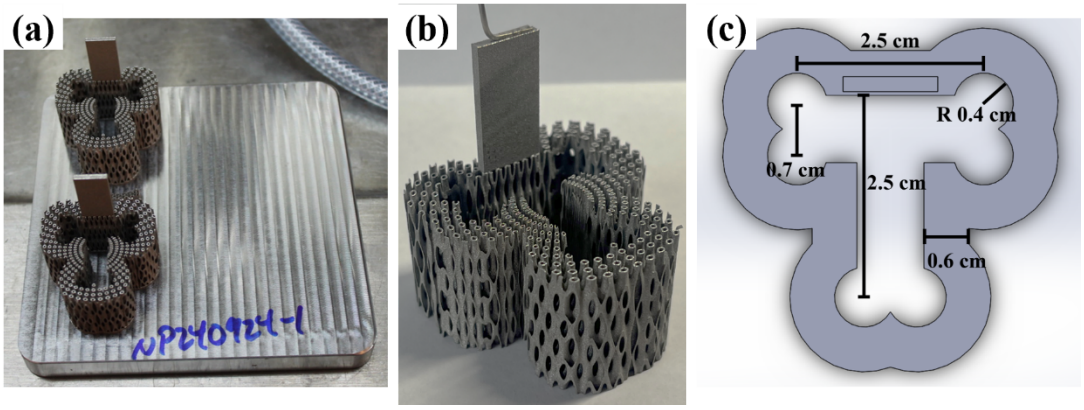

Figure 19. Selective Cathode (a) image on the build-plate, (b) image, and (c) schematic including measurements.

Subsequently, a stainless-steel wire was attached to the tab of the selective cathode with tack welds. The cathode was submerged in a 10 vol% nitric bath for 10 min to remove any contaminants prior to electropolishing. Figure 20 demonstrates the relative positioning of the anode and selective cathode during the electropolishing process. Using the selective cathode, the anodes were electropolished as described in chapter 2.

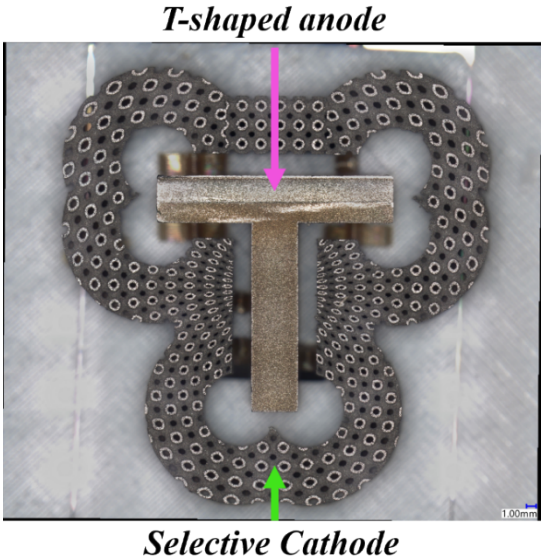

Figure 20. Image depicting the electrode spacing with the selective cathode.

Chapter 4 – Results

4.1: Reflectance

The following section presents reflectance measurements obtained from electropolished samples using various electrolytes, electrode spacings, and cathode geometries. Reflectivity measurements were obtained as a time-effective method to quantify electropolishing quality by measuring changes in surface brightness. Reflectance measurements were taken exclusively on the back surface of polished T-shapes, as illustrated in Figure 9. It should be noted that the selective cathode was tested only at an electrode spacing of 2 mm and should therefore be solely compared to cathode geometries at the 2 mm spacing.

4.1.1: Reflectivity of PEG-based electrolyte

Table 7 presents the increase in reflectivity values averaged in the visible spectrum (380 nm – 700 nm) before and after electropolishing in the PEG-based electrolyte, using various cathode geometries at different electrode spacings. The flat cathode samples exhibited the lowest increase in reflectivity amongst all cathode geometries at both electrode spacings, indicating poor brightening of the surface. This is attributed to the lack of cathode proximity on the back surface where reflectance measurements were taken, as the back surface is the furthest from the flat cathode (Figure 14). The selective cathode samples showed considerably greater reflectivity results compared to the flat, cylindrical, and conformal cathodes at the closer 2 mm spacing. This improvement is attributed to better control of electrode spacing (lessons learned during the first set of electropolishing work on how to mount the anode and cathode), leading to more uniform current distributions and effective polishing. The change in

reflectivity for all cathode geometries decreased at the larger electrode spacing suggesting that an increased spacing negatively affects the brightening of surfaces electropolished in the PEG-based electrolyte.

Table 7. Increase of reflectivity from as-printed to electropolished back surfaces using the PEG electrolyte		
	2 mm spacing	**20 mm spacing**
Flat Cathode	+ 3.64 %	+ 1.87 %
Cylindrical Cathode	+ 16.95 %	+ 15.98 %
Conformal Cathode	+ 17.38 %	+ 16.09 %
Selective Cathode Trial 1	+ 28.82 %	-
Selective Cathode Trial 2	+ 25.84 %	-

4.1.2: Reflectivity of acid-based electrolyte

presents the increase in reflectivity values averaged in the visible spectrum (380 nm – 700 nm) before and after electropolishing in the acid-based electrolyte, using various cathode geometries at different electrode spacings. The increase in reflectivity values were more uniform at the closer 2 mm spacing in the acid-based electrolyte than the PEG-based electrolyte. The flat cathode produced significantly higher reflectivity results in the acid-based electrolyte than in the PEG-based electrolyte, which is indicative of the lower sensitivity to cathode geometries in the acid-based electrolyte. The cylindrical and conformal cathode samples experienced an increase in reflectivity as the electrode spacing increased, which is contrary to the results from the PEG-based electrolyte.

presents the increase in reflectivity values averaged in the visible spectrum (380 nm – 700 nm) before and after electropolishing in the acid-based electrolyte, using various cathode geometries at different electrode spacings. The increase in reflectivity values were more uniform at the closer 2 mm spacing in the acid-based electrolyte than the PEG-based electrolyte. The flat cathode produced significantly higher reflectivity results in the acid-based electrolyte than in the PEG-based electrolyte, which is indicative of the lower sensitivity to cathode geometries in the acid-based electrolyte. The cylindrical and conformal cathode samples experienced an increase in reflectivity as the electrode spacing increased, which is contrary to the results from the PEG-based electrolyte.

Table 8. Increase of reflectivity from as-printed to electropolished back surfaces using the acid electrolyte.

	2 mm spacing	**20 mm spacing**
Flat Cathode	+ 32.49 %	+ 23.95 %
Cylindrical Cathode	+ 35.27 %	+ 38.00 %
Conformal Cathode	+ 33.74 %	+ 35.71 %
Selective Cathode Trial 1	+ 31.46 %	-
Selective Cathode Trial 2	+ 38.39 %	-

4.1.3: Electrolyte Comparison

Figure 21 shows the reflectivity of the back surfaces of T-shapes (Figure 9) electropolished with different electrode spacings in the PEG-based electrolyte (Figure 21a-c) and the acid-based electrolyte (Figure 21d-f). The acid-based electrolyte produced consistently brighter surfaces, with reflectivity values approximately 1.5 times as high as those produced with the PEG-based electrolyte across all cathode geometries and electrode spacings. This indicates that the acid-based electrolyte is more effective at increasing surface brightness when compared to the PEG-based electrolyte. Additionally, the acid-based electrolyte demonstrated more consistent reflectivity results regardless of cathode geometry. This suggests that the acid-based electrolyte is less sensitive to variations in cathode design. However, the reflectivity results from the acid-based electrolyte demonstrate that the cylindrical and conformal cathode configurations produce brighter surfaces at larger electrode spacings, indicating they may be overly aggressive at closer distances.

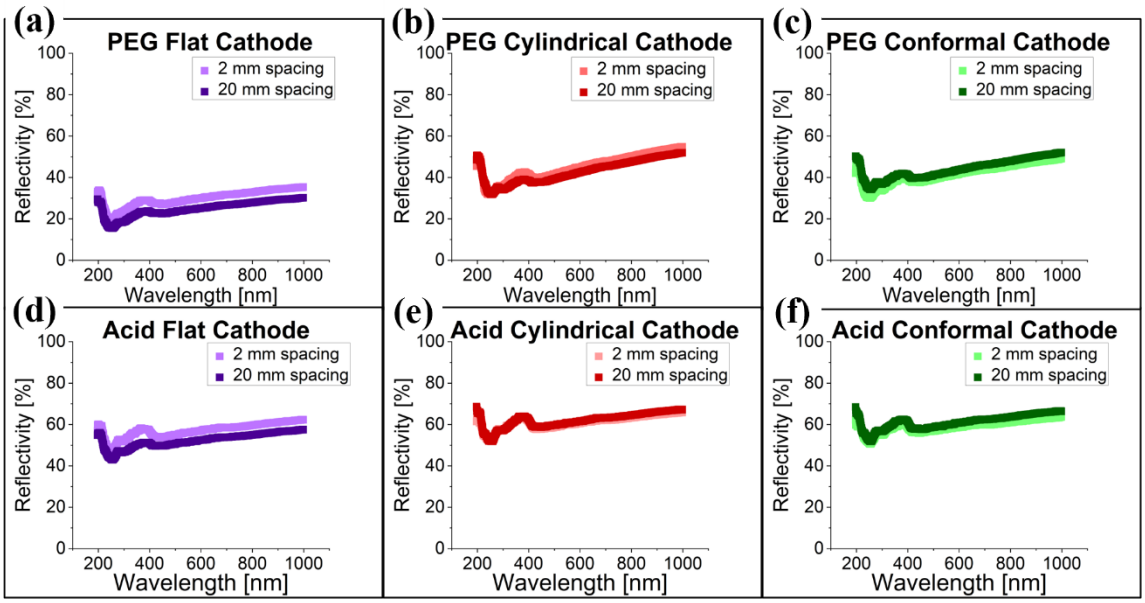

Figure 21. Plots of reflectance values comparing electrode spacings for samples electropolished in either (a-c) the PEG-based or (d-f) acid-based electrolyte.

4.2: Optical Images

The following section presents observations from optical images taken at 200x magnification of various orientations of as-printed and electropolished T-shaped samples, including front, back, left, and left-wall surfaces. The images illustrate the effects and morphological differences between surfaces electropolished with different electrolytes (PEG-based and acid-based), electrode spacings (2 mm and 20 mm), and cathode geometries (flat, cylindrical, conformal, and selective). These observations highlight differences in surface quality and uniformity achieved with each electropolishing configuration. Figure 22 depicts as-printed surfaces for each surface orientation (all surfaces were printed to be perpendicular to the build direction and therefore appear

similar optically in the as-printed state).

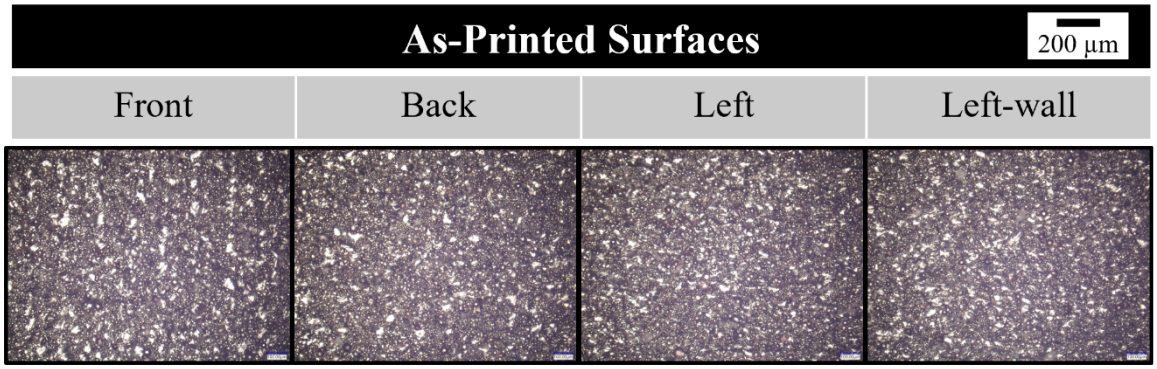

Figure 22. Optical images of as-printed surfaces for each surface orientation.

4.2.1: Front Surfaces

Figure 23 illustrates the optical images of the electropolished "front" surfaces (Figure 10a) of the T-shaped samples, utilizing different electrolytes, cathode geometries, and electrode spacings. In the PEG-based electrolyte, the flat cathode at the 2 mm electrode spacing was the only configuration to produce a reflective surface. Surface streaking, attributed to flow, was observed for the flat cathode at the 20 mm spacing and the cylindrical cathode at the 2 mm spacing. It should be noted that the imaging area was standardized for all samples (Figure 10a), and streaking was observed only in specific portions of the surface, not across the entire surface. The conformal and selective cathodes produced relatively smooth surfaces with occasional pitting.

Front surfaces polished in the acid-based electrolyte exhibited consistent results across all configurations, with varying densities of dimpling on the surface. At the 2 mm spacing, the dimpling density increases with the conformity of the cathode, progressing from flat to cylindrical to conformal to selective. Overall, the surfaces are more uniform and reflective in the acid-based electrolyte compared to the PEG-based electrolyte.

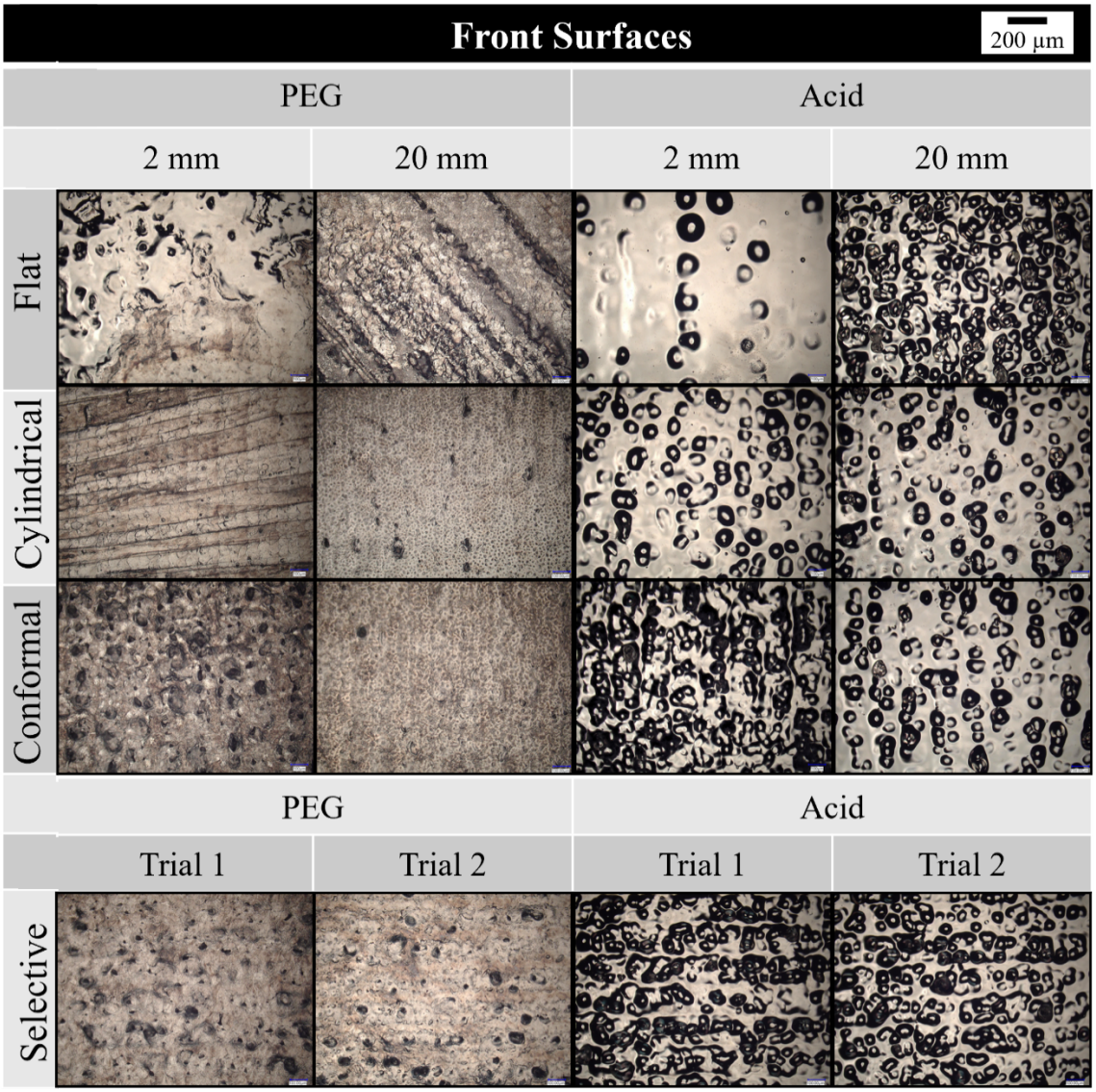

Figure 23. Spread of microscopic optical images of electropolished front surfaces.

4.2.2: Back Surfaces

Figure 24 illustrates the optical images of the electropolished "back" surfaces (Figure 10d) of the T-shaped samples. The overarching trends between the two electrolytes were similar. The following observations were drawn from the data for both electrolytes. In the PEG-based electrolyte, the flat cathode at both electrode spacings appeared minimally polished, which is attributed to the lack of cathode proximity on the back surface. A similar unpolished appearance was noted for the flat cathode at the 20

mm spacing in the acid-based electrolyte. The selective cathode produced the most uniform and smooth back surfaces of those polished with the PEG-based electrolyte. The 2 mm spacing for the cylindrical and conformal cathodes appeared rougher than their 20 mm spacing counterparts in both electrolytes. Overall, the back surfaces exhibited the roughest appearances among all configurations across all anode surfaces polished with either electrolyte.

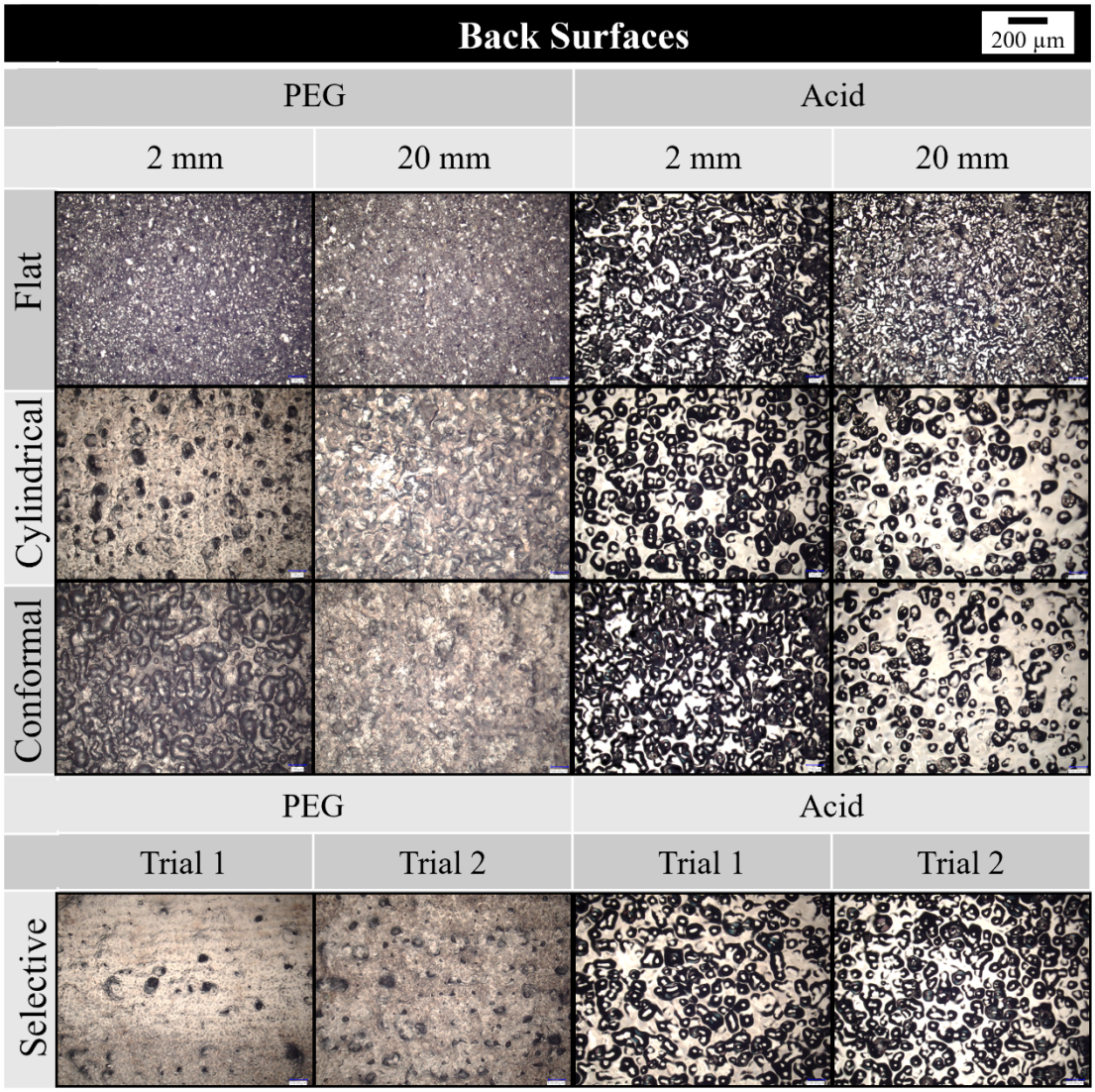

Figure 24. Spread of microscopic optical images of electropolished back surfaces.

4.2.3: Left Surfaces

Figure 25 illustrates the optical images of the electropolished “left” surfaces (Figure 10c) of the T-shaped samples. Left surfaces polished with the flat cathode in the PEG-based electrolyte exhibited similar behavior to back surfaces, appearing minimally polished due to the lack of cathode proximity. The PEG-based electrolyte resulted in several smooth surfaces, including the conformal cathode at the 2 mm spacing, the cylindrical cathode at both electrode spacings, and the selective cathode. In the acid-based electrolyte, surfaces polished with the cylindrical cathode at both electrode spacings and the conformal cathode at the 20 mm spacing exhibited less dimpling and more uniformity. Overall, the left surface exhibited the smoothest appearances among all configurations across all anode surface polished in either electrolyte.

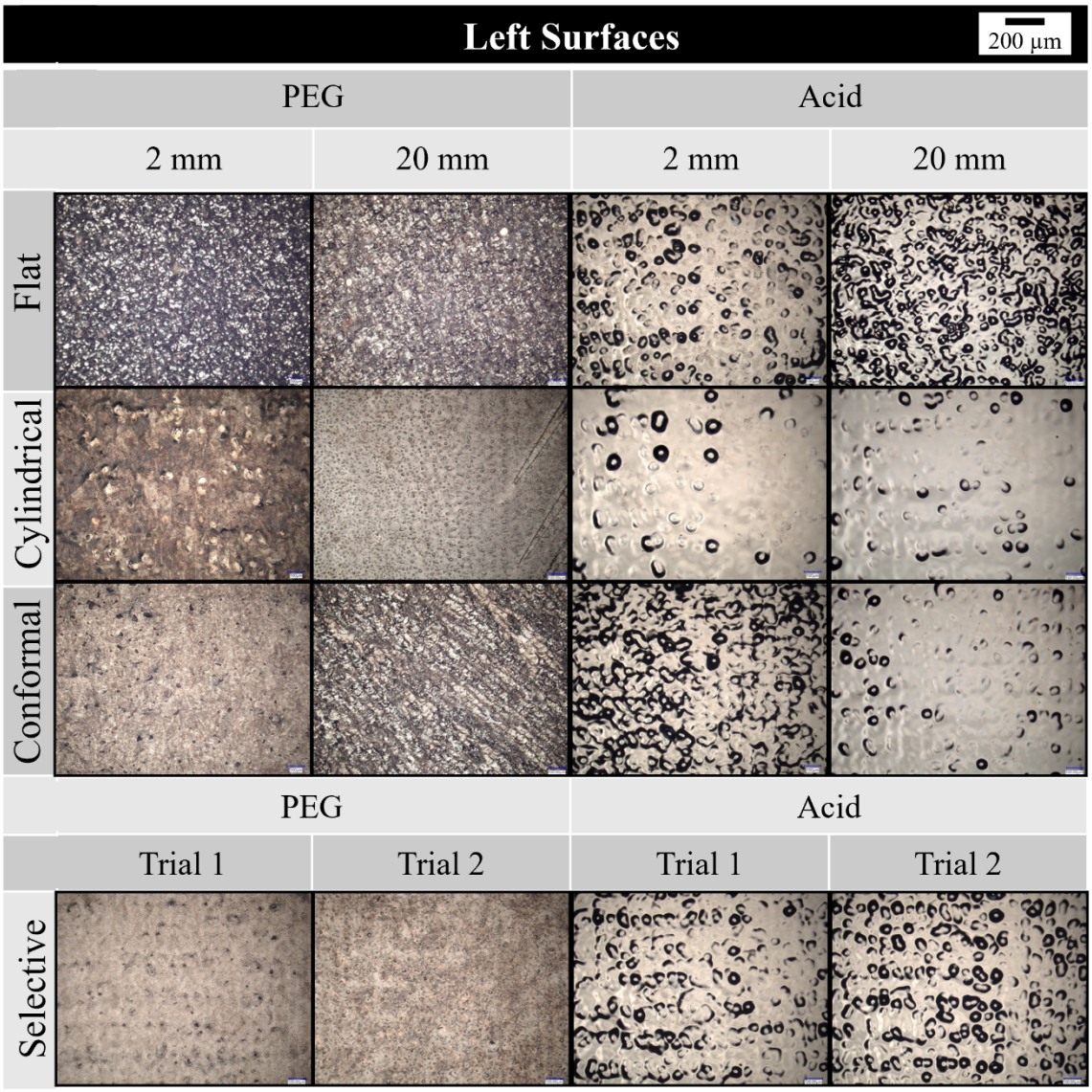

Figure 25. Spread of microscopic optical images of electropolished left surfaces.

4.2.4: Left-wall Surfaces

Figure 26 illustrates optical images of the electropolished "left-wall" surfaces (Figure 10b) of the T-shaped samples. Several configurations of the PEG-based electrolyte exhibited minimally polished appearances, including the flat and cylindrical cathodes at both electrode spacings and the conformal cathode at the 20 mm spacing. This indicates the limited electropolishing effect of the PEG-based electrolyte on surfaces furthest from the cathode. The selective cathode produced the smoothest appearing

surfaces among those polished with the PEG-based electrolyte, with some surface streaking attributed to flow. The left-wall surfaces polished in the acid-based electrolyte exhibited smoother appearances than the front and back surfaces. The cylindrical and conformal cathodes at the 20 mm spacing produced the smoothest appearing left-wall surfaces among those polished in the acid-based electrolyte.

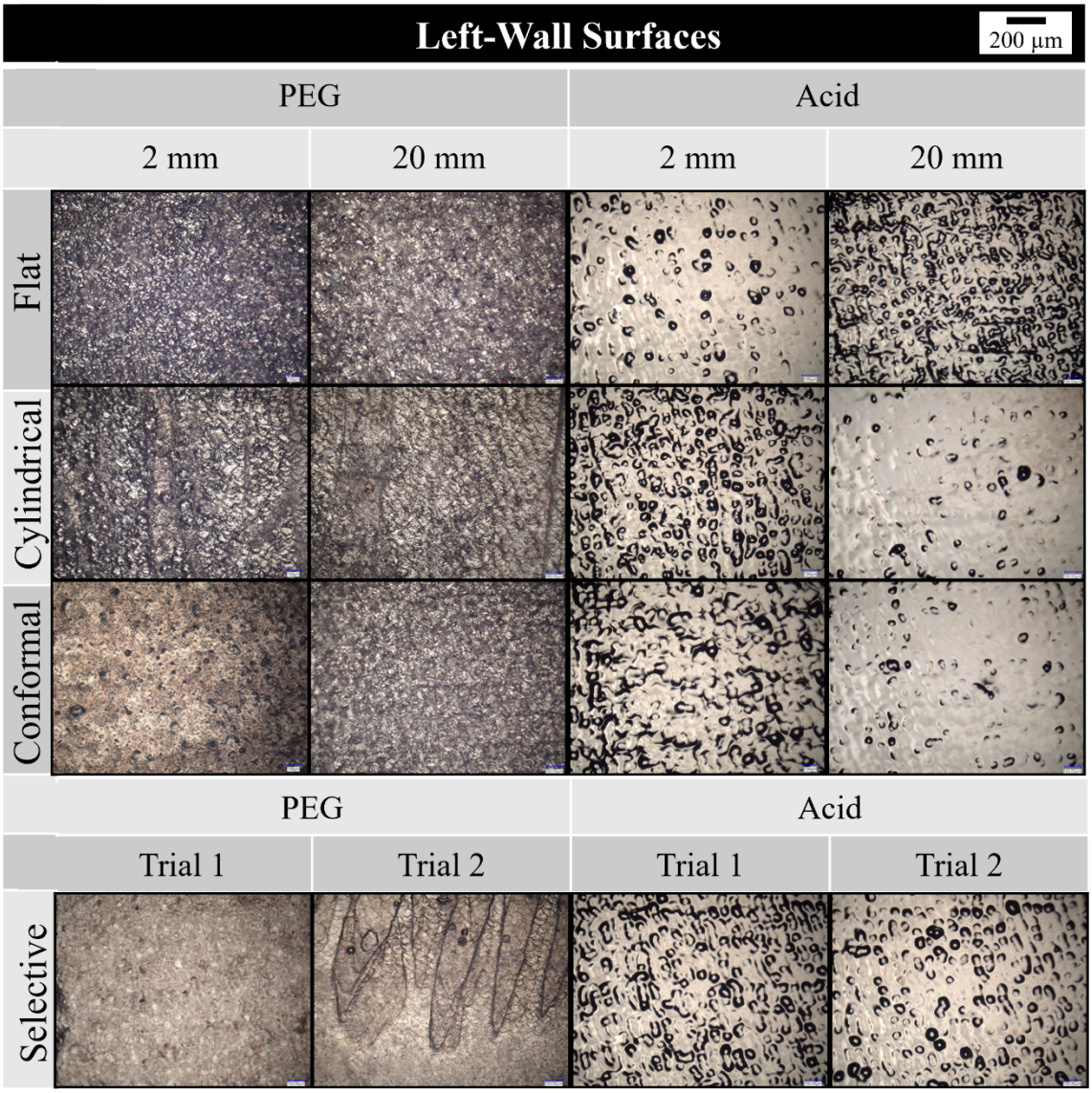

Figure 26. Spread of microscopic optical images of electropolished left-wall surfaces.

4.2.5: Summary

The optical images reveal differences among the front, back, left, and left-wall surfaces of T-shaped samples, as well as between PEG-based and acid-based electrolytes. The front and back surfaces generally appeared rougher than the left and left-wall surfaces across both electrolytes. The acid-based electrolyte consistently produced more uniform and reflective surfaces across all configurations, with less sensitivity to cathode geometry and electrode spacing. In contrast, the PEG-based electrolyte exhibited greater variability, with certain configurations showing minimal polishing or surface streaking. The selective cathode generally produced the smoothest surfaces in the PEG-based electrolyte, while the cylindrical and conformal cathodes at 20 mm spacing yielded the best results in the acid-based electrolyte. Overall, the acid-based electrolyte created more reflective and uniform surfaces than the PEG-based electrolyte.

4.3: Surface Roughness

The following sections compare roughness data between the “front”, “back”, “left”, and “left-wall” surfaces of electropolished T-shape samples in both the PEG-based and acid-based electrolyte. Surface roughness is characterized through S_a (arithmetic mean height) measurements. The measurement is collected as a mean plane is established over a specific area and the average height of the surface profile is calculated.

4.3.1: Front Surfaces

Figure 27a illustrates the surface roughness values for “front” surfaces of T-shaped samples before and after electropolishing, using various cathode geometries and electrode spacings in the PEG-based electrolyte. Among all the samples electropolished in the PEG-based electrolyte, the flat cathode at the 2 mm spacing resulted in the highest

surface roughness. In contrast, samples polished with the cylindrical cathode exhibited consistently low surface roughness values in the PEG-based electrolyte.

Figure 27b depicts surface roughness data for "front" surfaces electropolished in the acid-based electrolyte. Notably, the sample polished with the flat cathode at the 20 mm spacing exhibited one of the highest surface roughness values, whereas its 2 mm counterpart displayed one of the lowest values. The second trial of the selective cathode demonstrates the smoothest surface in the acid-based electrolyte. While the front surfaces electropolished with the acid-based electrolyte demonstrated the best consistency, those polished in the PEG-based electrolyte generally exhibited lower surface roughness values. Overall, surface roughness values were reduced for all electropolished front surfaces.

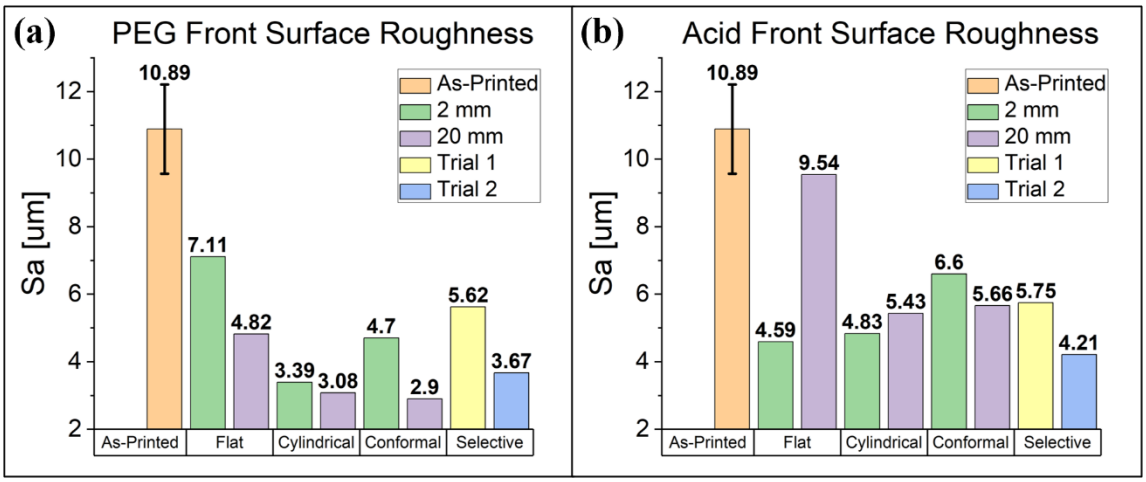

Figure 27. Plots of front surface roughness for samples electropolished with (a) the PEG-based electrolyte, and (b) the acid-based electrolyte.

4.3.2: Back Surfaces

Figure 28a depicts the surface roughness values for "back" surfaces electropolished in the PEG-based electrolyte. The surfaces electropolished with the flat cathode exhibited increased roughness compared to their initial state. This is attributed to

the lack of cathode proximity, as the back surface is not directly aligned with the flat cathode. All other cathode geometries significantly reduced the initial surface roughness, except for the conformal cathode at the 2 mm spacing.

Figure 28b depicts the surface roughness values for "back" surfaces electropolished in the acid-based electrolyte. The back surfaces exhibited similar behavior to the front surfaces, with samples electropolished in the acid-based electrolyte producing consistent results across all parameters. However, back surfaces electropolished in the PEG-based electrolyte generally had lower surface roughness values. Notably, the back surface had the highest initial surface roughness among all sides, which was significantly reduced after electropolishing.

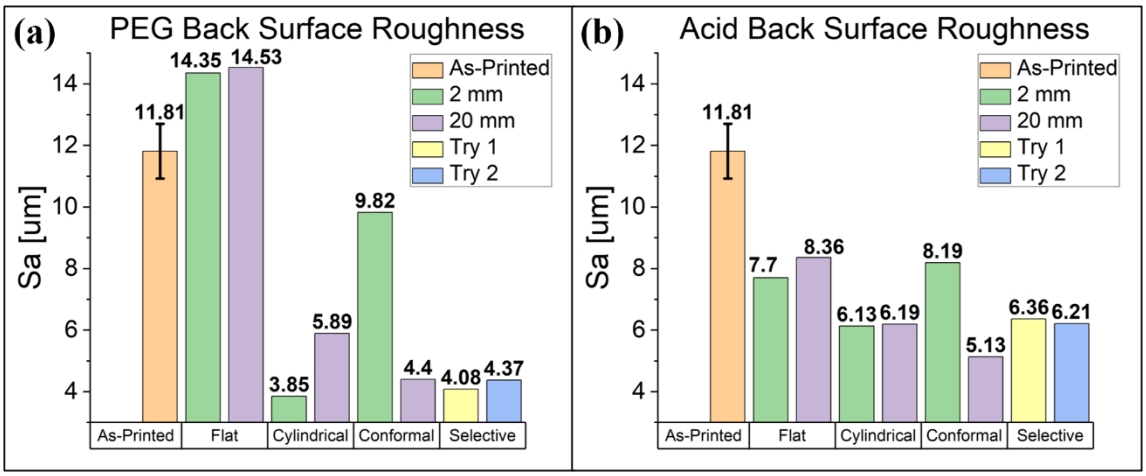

Figure 28. Plots of back surface roughness for samples electropolished with (a) the PEG-based electrolyte, and (b) the acid-based electrolyte.

4.3.3: Left Surfaces

Figure 29 illustrates the surface roughness values for "left" surfaces electropolished in both the PEG-based and acid-based electrolyte. Among the samples electropolished in the PEG-based electrolyte, the flat cathode at the 20 mm spacing notably became rougher than its initial state. The other cathodes performed consistently

and significantly reduced the initial surface roughness, except for the flat cathode at the 2 mm spacing and the conformal cathode at the 20 mm spacing. The left surfaces polished in the acid-based electrolyte also demonstrated excellent performance, showing both consistency and overall surface roughness reduction. Among all surfaces, the left surface is one of the few where the acid-based electrolyte performed more consistently at reducing surface roughness across all parameters compared to the PEG-based electrolyte. Overall, the left surface exhibited some of the lowest initial surface roughness values amongst all orientations.

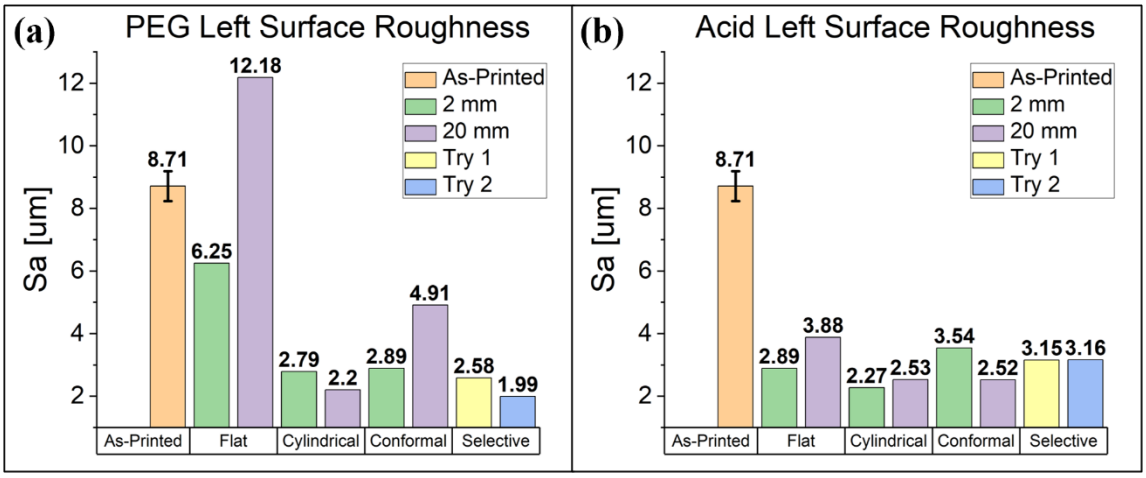

Figure 29. Plots of left surface roughness for samples electropolished with (a) the PEG-based electrolyte, and (b) the acid-based electrolyte.

4.3.4: Left-wall Surfaces

Figure 30 illustrates the surface roughness values for "left-wall" surfaces electropolished in both the PEG-based and acid-based electrolyte. Among the samples electropolished in the PEG-based electrolyte, the flat cathode at the 20 mm spacing stands out for its minimal reduction in surface roughness, performing notably worse compared to other samples. All other left-wall surfaces electropolished in the PEG-based and acid-based electrolytes performed consistently with significant reductions in initial

surface roughness. Overall, the electropolished left-wall surfaces exhibit considerably reduced final surface roughness compared to front and back surfaces.

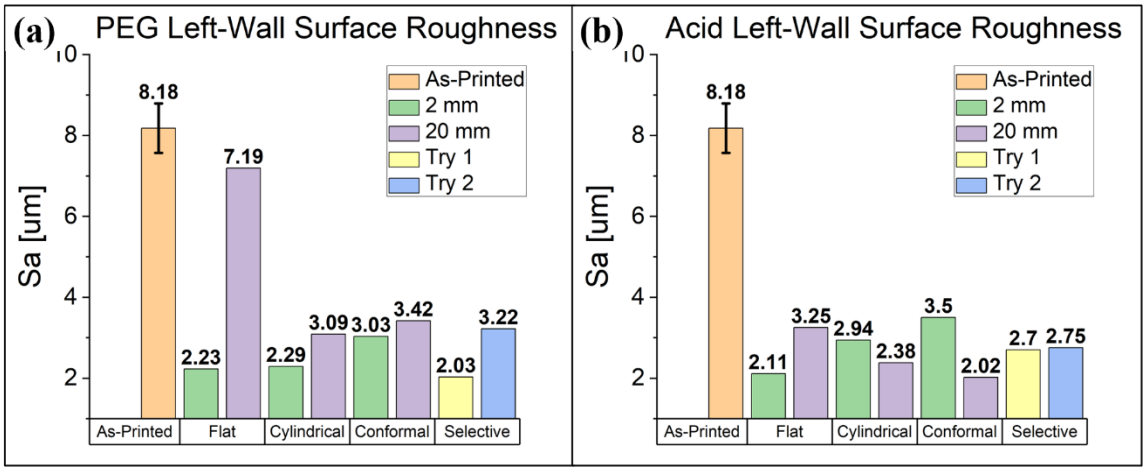

Figure 30. Plots of left-wall surface roughness for samples electropolished with (a) the PEG-based electrolyte, and (b) the acid-based electrolyte.

4.3.5: Summary

Overall, the acid-based electrolyte generally yielded more consistent results across all parameters when compared to the PEG-based electrolyte. However, the PEG-based electrolyte produced lower surface roughness values when compared to the acid-based electrolyte on the front and back surfaces, while the left and left-wall surfaces showed more consistent values for both electrolytes. Among the various cathode geometries, the cylindrical cathode produced the most consistent results on the surfaces in both electrolytes. The front and back surfaces generally exhibited higher final surface roughness values than the left and left-wall surfaces, with the left surfaces exhibiting the lowest final surface roughness values across all parameters.

4.4: Mass Changes

Mass measurements were obtained before and after electropolishing T-shaped anodes. The results are organized by electrolyte type and include comparisons between

the PEG-based and acid-based electrolytes. Similarities were observed between the PEG-based and acid-based electrolytes. However, inconsistencies between applied current density values and mass changes were observed for samples electropolished in the acid-based electrolyte.

Table 9 and Table 10 demonstrate the changes in mass exhibited by samples electropolished using varying cathode geometries at different electrode spacings in the PEG-based and acid-based electrolyte, respectively. The overall mass loss for an individual electrolyte was similar between the 2 mm and 20 mm electrode spacings, except for the flat cathode, which exhibited significantly less removal at the 20 mm spacing in both electrolytes. Samples polished with the cylindrical cathode exhibited the highest material removal at both electrode spacings, potentially indicating a more targeted electropolishing effect at corners. At the closer electrode spacing, the flat cathode removed more material than the conformal cathode, while the opposite was true at the larger electrode spacing. This could be attributed to inadequate flow experienced by the conformal cathode at the closer electrode spacing.

Table 9. Mass loss for PEG-based electrolytes.

	2 mm spacing	**20 mm spacing**
Flat Cathode	0.643 g	0.463 g
Cylindrical Cathode	0.650 g	0.630 g
Conformal Cathode	0.514 g	0.617 g
Selective Cathode Trial 1	0.637 g	-
Selective Cathode Trial 2	0.634 g	-

Table 10. Mass loss for acid-based electrolytes		
	2 mm spacing	**20 mm spacing**
Flat Cathode	1.021 g	0.663 g
Cylindrical Cathode	1.140 g	1.132 g
Conformal Cathode	0.929 g	1.031 g
Selective Cathode Trial 1	0.964 g	-
Selective Cathode Trial 2	1.047 g	-

Although the two electrolytes demonstrated similar trends, there were notable differences in the behavior of both with relation to mass loss. For the flat cathode, the PEG-based electrolyte showed less variation in mass loss between the 2 mm and the 20 mm spacings compared to the acid-based electrolyte. The cylindrical cathode consistently showed the highest mass loss at both electrode spacings in both electrolytes, while the conformal cathode landed somewhere in between the two other cathodes.

Although the acid-based electrolyte removed more material than the PEG-based electrolyte, a direct correlation between the current density and material removal was expected. Samples electropolished in the acid-based electrolyte were subjected to a current density approximately 7 times higher than samples polished in the PEG-based electrolyte, yet only ~2 times more material removal was observed, suggesting significant losses in electropolishing efficiency for the acid-based electrolyte compared to the PEG.

4.5: Experimental and COMSOL Model 3D Profilometry

Profiles of the T-shaped anodes were acquired before and after electropolishing and compared to profiles from the COMSOL model. Electrode thickness changes were calculated by manually aligning the as-printed profiles with the electropolished profiles

for both the experimental and modeling results. Thickness changes between the profiles were calculated at three points on the surface, as shown in Figure 31. Point 1 (Figure 31a-b) measures the thickness change at the inner corner of the T-shaped anode. Thickness changes at the front corner are summarized by points 2 and 3 (Figure 31a,c) which describe horizontal and vertical thickness changes, respectively. Due to the manual alignment process and adjustments for tilt, inherent inaccuracies exist within the following data. It should be noted that the COMSOL model simplifies real-world physics, and although values obtained from the model are not 100% accurate, the developed model effectively captures the trends observed in the experimental results of the present study.

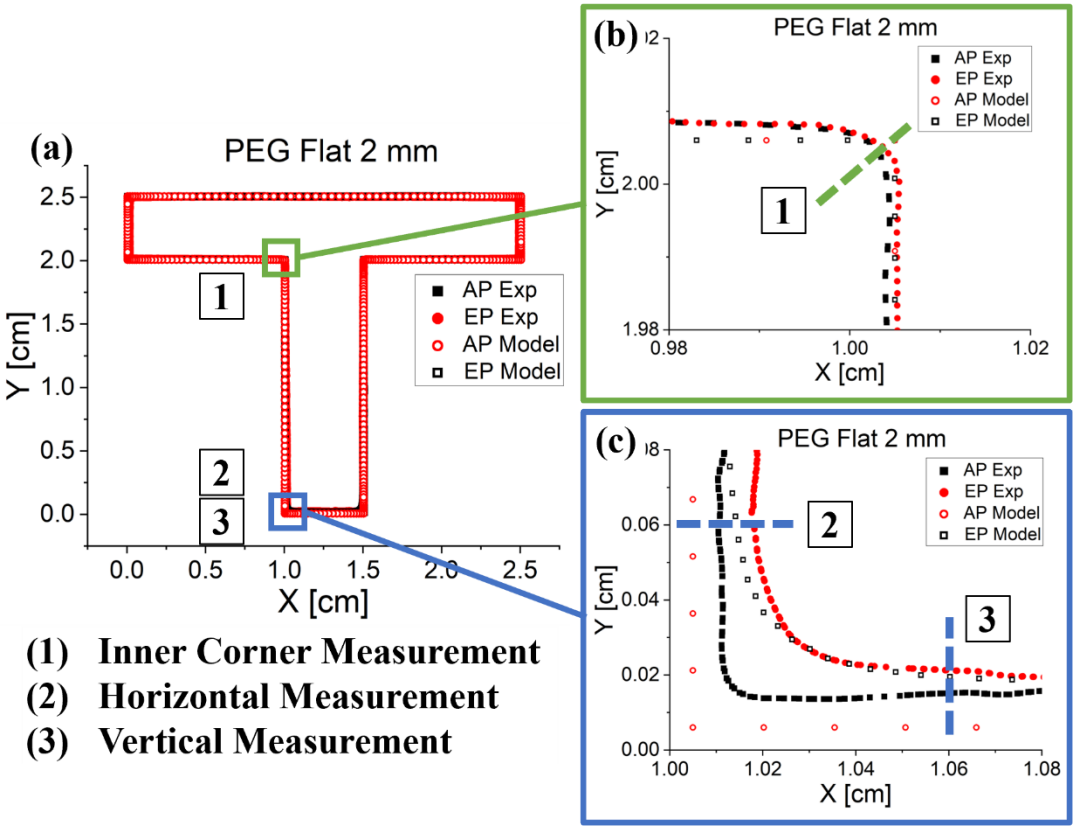

Figure 31. (a) Schematic of 3D profilometry measurements obtained from (b) inner corner and (c) front corner.

4.5.1: Front Corner (Points 2 and 3)

Experimental and modeling results from profile comparisons between the two electrode spacings in the PEG-based and acid-based electrolyte revealed the following trends. In both electrolytes, the experimental and model results for the flat cathode revealed greater thickness changes at the front corner (points 2 and 3 from Figure 31) for the closer 2 mm electrode spacing compared to the 20 mm spacing. These findings align with experimental mass change measurements, as the flat cathode removed approximately 0.2 g more material at the 2 mm spacing for the PEG-based electrolyte and 0.4 g more material for the acid-based electrolyte. This is likely due to a lack of cathode proximity at the further electrode spacing.

The experimental and modeling profile trends aligned for the cylindrical cathode results in both electrolytes, indicating greater thickness changes for the front corner (points 2 and 3 from Figure 31) at the larger 20 mm spacing. Although, experimental mass measurements for the cylindrical cathode at both electrode spacings in their respective electrolytes were quite similar, with a difference of only 0.02 g in the PEG-based electrolyte and 0.01 g in the acid-based electrolyte. The similarities in mass removal between both electrode spacings, as well as comparisons between 2D profiles (Figure 32 and Figure 33) suggest that the cylindrical cathode at the 20 mm spacing causes a concentration of current density at corners, resulting in targeted material removal in those areas. In comparison, the cylindrical cathode at the closer 2 mm spacing achieves more uniform current density distributions across the anodic surface, leading to consistent material removal rather than targeting the corners. The targeted electropolishing effect at the corners is much more exaggerated by the COMSOL model

with the acid-based electrolyte at the 20 mm spacing and does not accurately represent experimental results.

Experimental and modeling results obtained for the conformal cathode also indicate a greater thickness change at the front corner at the larger 20 mm spacing in both electrolytes. However, experimental mass change measurements demonstrated more material removal (approximately 0.1 g in both electrolytes) for the conformal cathode at the larger 20 mm spacing. Similar to the cylindrical cathode, results from the conformal cathode indicate a targeting electropolishing effect at corners. However, the differences in mass measurements between the two electrode spacings and comparisons between 2D profiles (Figure 32 and Figure 33) suggest that the targeting effect is not as pronounced as with the cylindrical cathode. The targeted electropolishing effect at the corners is much more exaggerated by the COMSOL model with the acid-based electrolyte at the 20 mm spacing and does not accurately represent experimental results.

4.5.2: Inner Corner (Point 1)

The COMSOL model struggled with accurately modeling the inner corner of the T-shaped anode, likely due to its sharp edge. Future considerations for developing the accuracy of the model look to modify the sharp edge into a more curve-like feature. Due to the issues of modeling the inner corner, changes between the as-printed and electropolished profiles always resulted in a negligible amount.

Experimental 2D profile results for the PEG-based electrolyte revealed the difficulties of effectively electropolishing the inner corner. In general, experimental results from the PEG-based electrolyte demonstrated negligible changes between the as-printed and electropolished profiles of the inner corner. The selective cathode was one of

the few exceptions, with a change in profiles of about 60 μm. On the other hand, experimental results from the acid-based electrolyte revealed significant changes to the inner corner. However, it should be noted that the acid-based samples presented greater challenges in aligning profiles, which may have introduced some inaccuracies. The conformal cathode produced the most significant thickness changes for the inner corner among all cathodes at both electrode spacings. Both the flat and conformal cathode experienced greater changes at the larger electrode spacing compared to the closer electrode spacing. In contrast, the cylindrical cathode produced a greater change to the inner corner at the closer electrode spacing. The selective cathode was the only cathode to produce negligible changes between AP and EP profiles in the acid-based electrolyte.

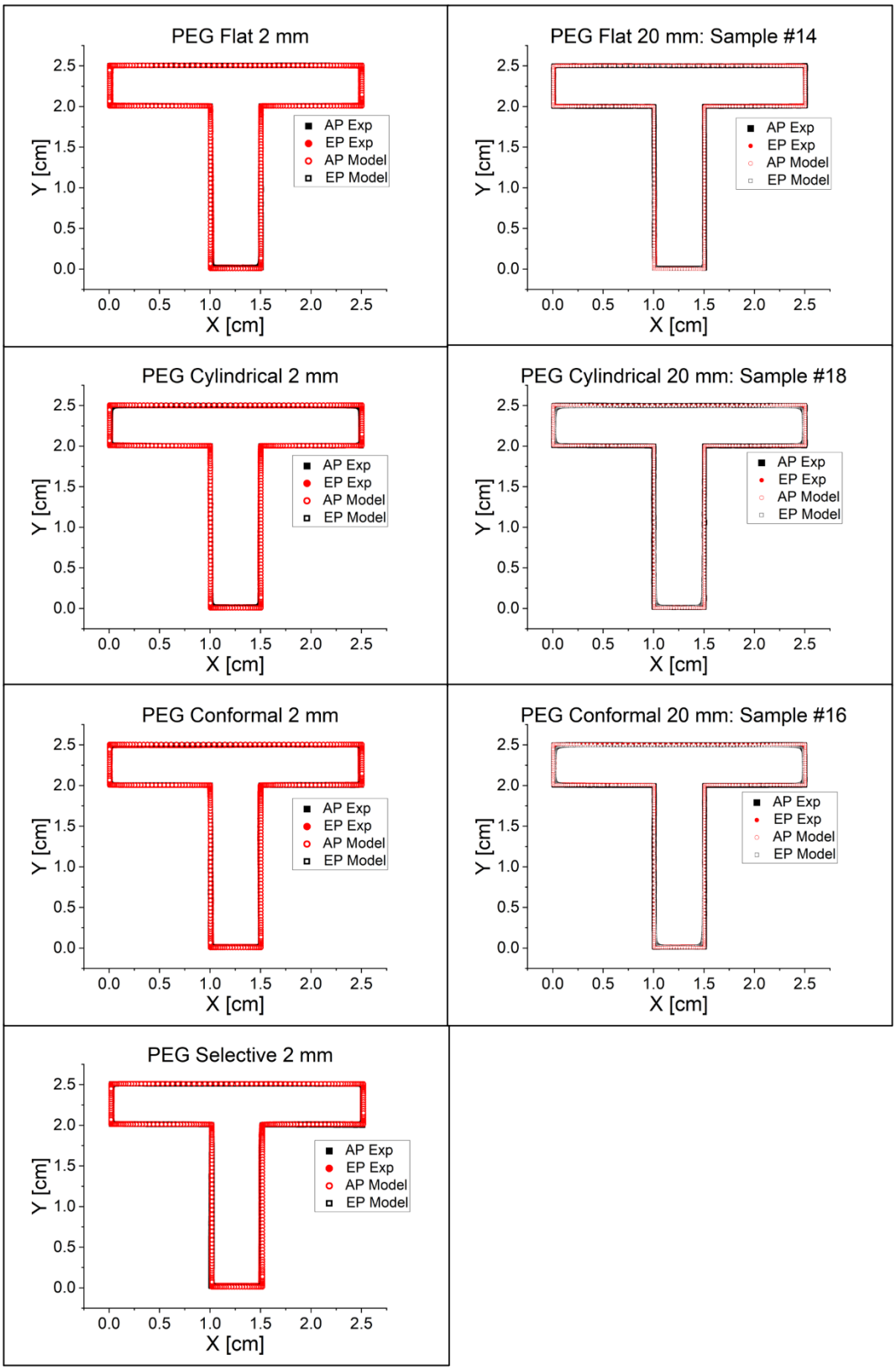

Figure 32. Plots of profilometry results modeling the PEG-based electrolyte.

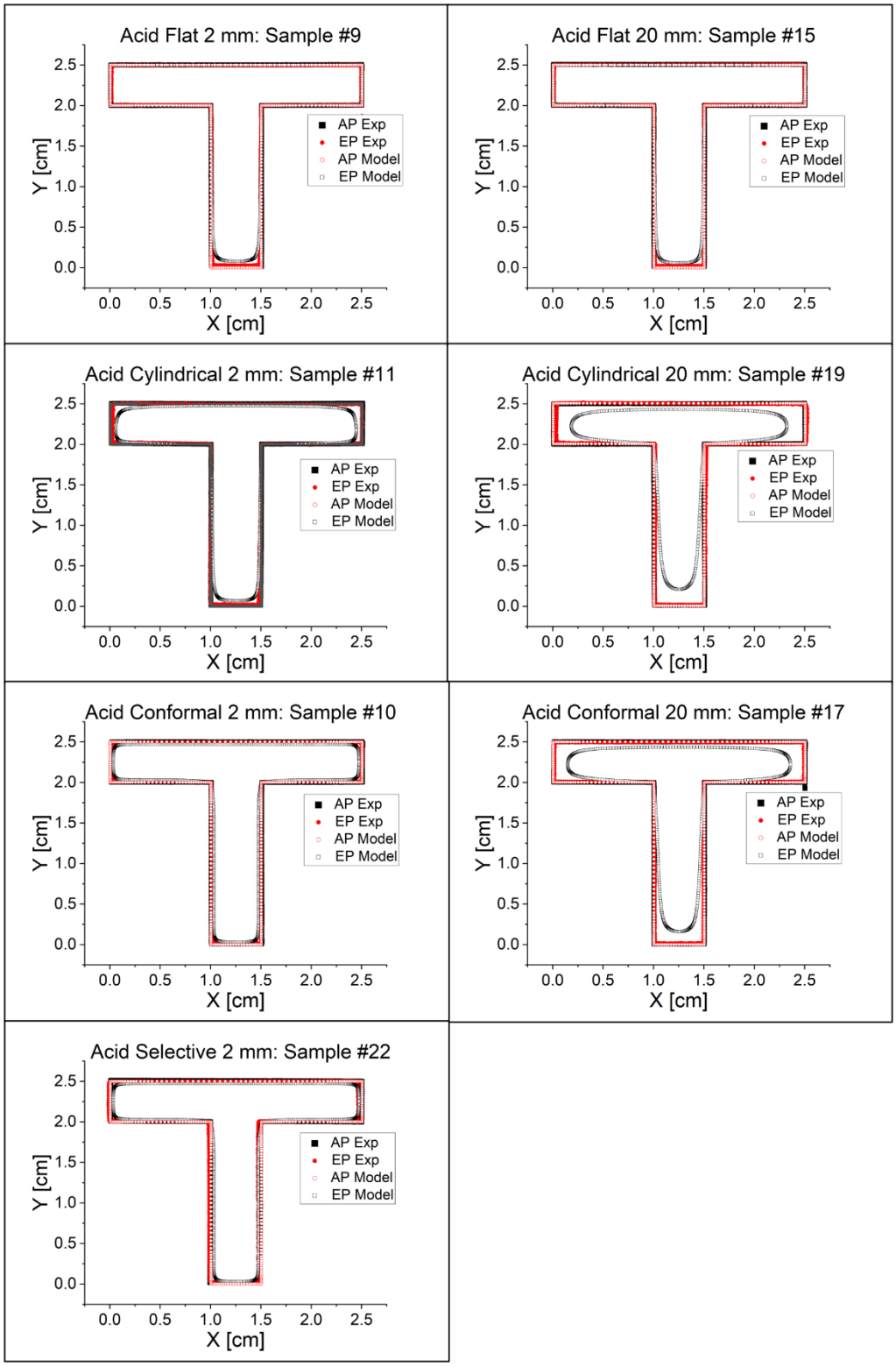

Figure 33. Plots of profilometry results modeling the acid-based electrolyte.

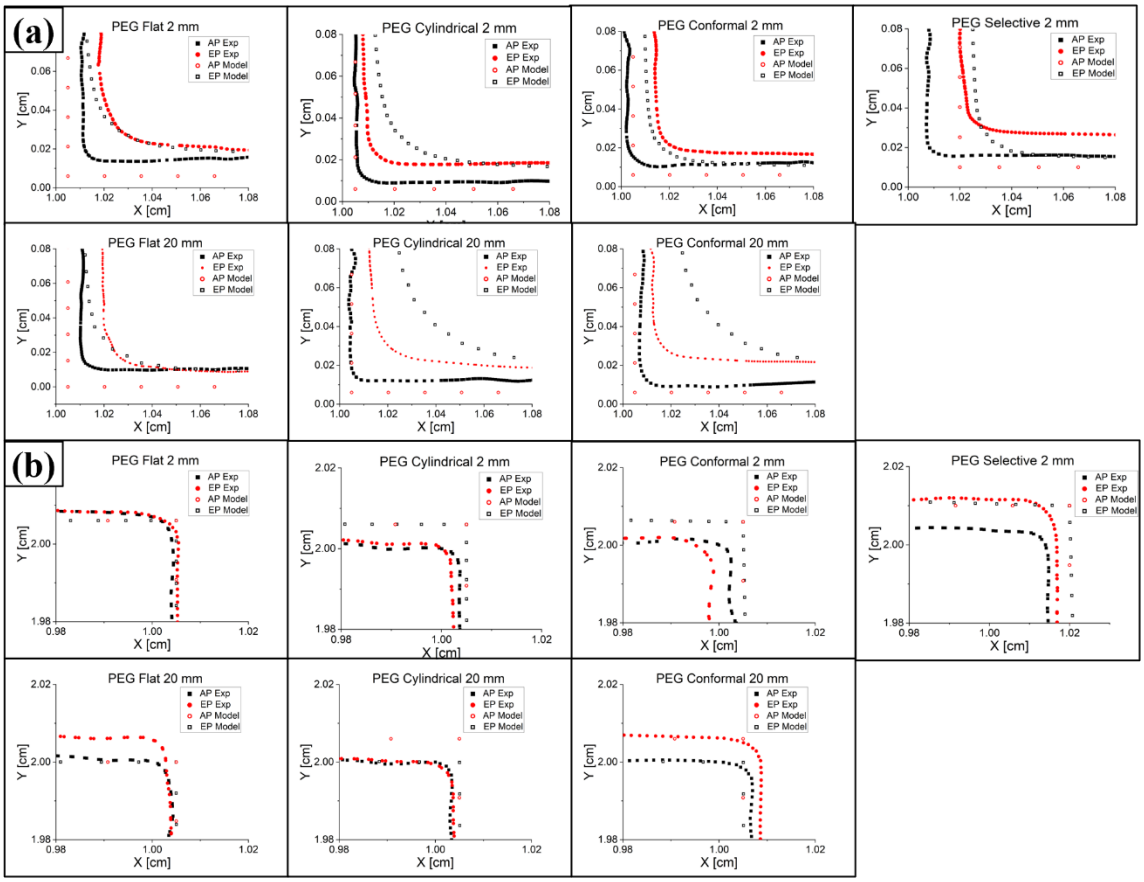

Figure 34. Plots of profilometry results modeling the PEG-based electrolyte at (a) the front corner, and (b) the inner corner.

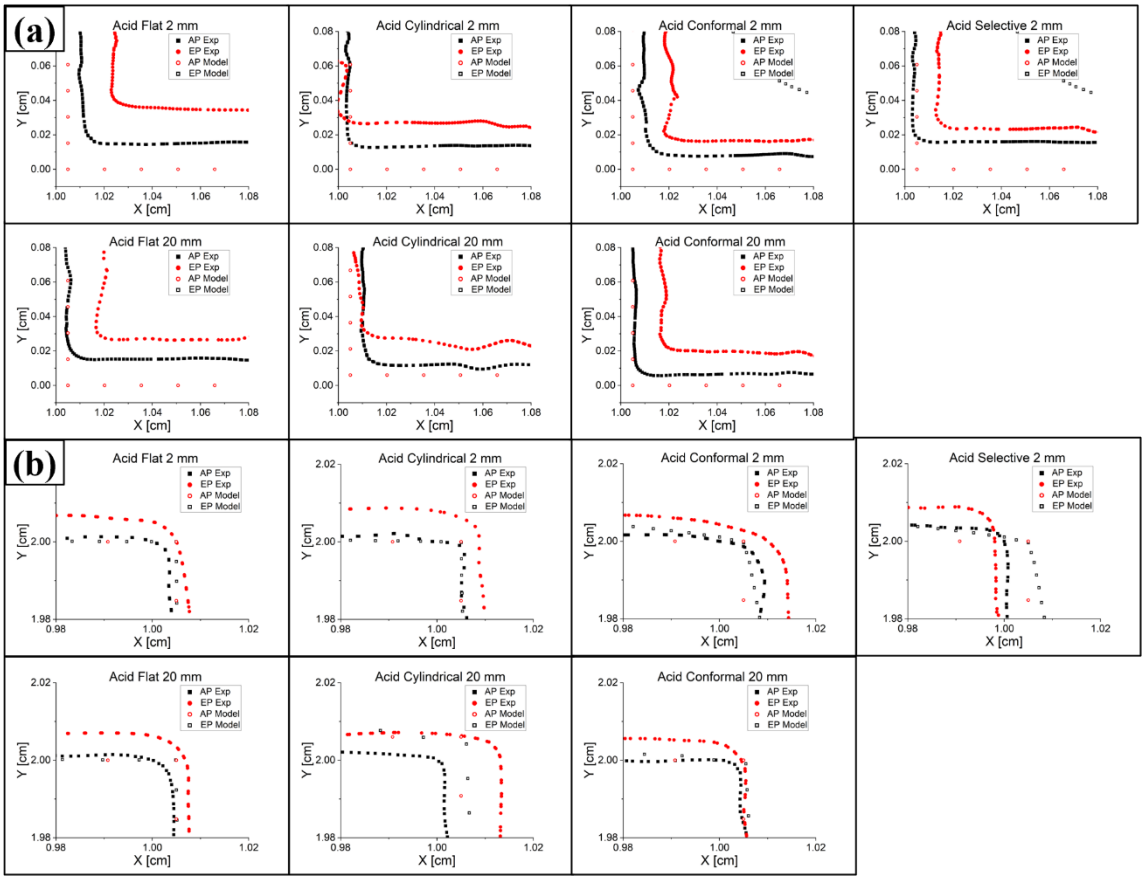

Figure 35. Plots of profilometry results modeling the PEG-based electrolyte at (a) the front corner, and (b) the inner corner.

4.5.3: Material Removal Uniformity

Averages and standard deviations were calculated from the distances obtained from 2D profilometry for all three points of interest (Figure 31) from both experimental and model results. At each point of interest (inner corner, horizontal, and vertical) the difference in distances between the expected model and actual experimental results were also calculated. Similar average and standard deviations were then determined to inform about discrepancies between the model and experimental results. Table 11 and Table 12 contain the average and standard deviation results for the PEG-based and acid-based electrolyte, respectively.

As previously mentioned, the COMSOL model simplifies real-world physics, and although values from the model are not 100% accurate, it is able to effectively capture trends observed in experimental results of the present study. As a result, average values from the model seen in Table 11 and Table 12 are not expected to accurately represent what to expect from the experimental values. However, the standard deviation calculations for both experimental and model results give us an idea of the degree of uniform material removal at the three points of interest. Lower standard deviations indicate more uniform material removal, while higher standard deviations suggest less uniformity (large differences between material removal at the inner corner, horizontal, and vertical surfaces). Similarly, standard deviation calculations of the differences between the model and experimental results indicate the degree of alignment between the two. Lower standard deviations suggest a closer match between the model and experimental outcomes at the three points of interest.

In the PEG-based electrolyte, the selective cathode resulted in the lowest standard deviations for experimental and model results, indicating the most uniform material removal amongst all cathode geometries. This suggests that the selective cathode is performing as intended, as it was designed to create the most uniform current distributions across the anodic surface, thereby achieving the most uniform material removal. The selective cathode also resulted in the lowest standard deviation values for differences between experimental and model results for both electrolytes, as outlined in Table 11 and Table 12, suggesting that the selective cathode achieved the best alignments between experimental and model results among all cathode geometries.

Table 11. Material removal averages and standard deviations in the PEG electrolyte from all horizontal, vertical, and inner corner measurements.							
	Spacing	Experimental		Model		Difference	
		Average [µm]	Standard Dev. [µm]	Average [µm]	Standard Dev. [µm]	Average [µm]	Standard Dev. [µm]
Flat Cathode	2 mm	49.1	28.5	57.1	57.1	30.6	32.3
	20 mm	26.7	37.7	60.1	43.0	33.5	45.7
Cylindrical Cathode	2 mm	42.0	36.9	63.1	50.3	21.1	15.0
	20 mm	59.2	41.8	121	86.2	61.4	45.3
Conformal Cathode	2 mm	49.8	39.0	33.9	24.4	15.9	23.8
	20 mm	67.9	32.2	121	86.2	52.7	74.9
Selective Cathode	2 mm	93.6	24.2	31.4	22.2	62.2	3.78

Table 12. Material removal averages and standard deviations in the acid electrolyte from all horizontal, vertical, and inner corner measurements.							
	Spacing	Experimental		Model		Difference	
		Average [µm]	Standard Dev. [µm]	Average [µm]	Standard Dev. [µm]	Average [µm]	Standard Dev. [µm]
Flat Cathode	2 mm	123	58.9	462	412	339	357
	20 mm	96.6	24.8	411	310	315	289
Cylindrical Cathode	2 mm	62.8	53.4	508	402	445	378
	20 mm	83.1	38.4	827	685	744	649
Conformal Cathode	2 mm	81.2	21.4	217	154	135	137
	20 mm	124.9	44.3	1080	877	960	906
Selective Cathode	2 mm	65.76	47.58	246.33	174.20	180.56	128.33

Chapter 5 – Discussion

5.1: Reflectivity, Optical, Roughness, and Electrolyte Comparisons

5.1.1: Electrode Spacings

Miniscule differences were noted in general roughness changes for most cathode geometries in both electrolytes at the two different electrode spacings (2 and 20 mm). However, the flat cathode geometry demonstrated a clear impact between the two electrode spacings. At the further 20 mm spacing, samples electropolished with the flat cathode in either electrolyte exhibited significantly less mass loss than at the 2 mm spacing. Similarly, the 20 mm spacing produced larger roughness values on all faces except the front when compared to the 2 mm spacing. The impact of electrode spacing on results obtained with the flat cathode are attributed to the lack of cathode proximity which has been shown to affect current density distributions [78]. The results of the present study are corroborated by several studies that have outlined the impact of closer electrode spacings on improvements to surface roughness reductions [8, 9, 11, 64, 78].

In the acid-based electrolyte, reflectivity values measured on the back surface saw an increase as the electrode spacing increased for both the cylindrical and conformal cathodes. This was corroborated by optical images which demonstrated a slight decrease in dimpling density from the 2 mm to the 20 mm spacing for the cylindrical and conformal cathodes. In the PEG-based electrolyte, reflectivity was slightly higher at the closer 2 mm spacing for all cathode geometries, although the increase was almost negligible. Overall, no clear trends emerged to describe the effect of electrode spacing, indicating that cathode geometry played a more significant role in determining electropolishing results.

5.1.2: Electrolyte Consistency

Results from optical images, reflectivity and roughness measurements concluded that the acid-based electrolyte produced more consistent and repeatable surfaces regardless of cathode geometry and spacing, whereas the PEG-based electrolyte was more sensitive those factors. The standard deviation of both reflectivity changes and roughness values for samples electropolished in the PEG-based electrolyte were up to twice as high as those in the acid-based electrolyte, indicating a more consistent spread in data for the acid-based electrolyte (excluding the flat cathode values). The consistency of samples electropolished in the acid-based electrolyte was also demonstrated in optical images. The acid-based electrolyte produced bright surfaces with dimpled surface features regardless of the other parameters. The dimpling of the surface can be caused by two predominate factors: either the selected current (14 A) did not generate a large enough current density to get the entire anode surface into the polishing regime, resulting in an etching-type phenomenon [7, 62-64, 66] or the gas evolution at the anode surface creates local areas of shielding that can generate these dimples [7, 87].

Meanwhile, the PEG-based electrolyte demonstrated a higher sensitivity to electropolishing parameters, as seen through the myriad of morphologies observed in the optical images, such as streaking, variations in color and brightness, and remnants of the original surface. The PEG-based electrolyte's sensitivity to cathode geometry is evident from the poor performance of the flat cathode in terms of reflectance and roughness results when compared to the acid-based electrolyte. Generally, the selective cathode performed well in both the PEG-based and acid-based electrolyte through increased reflectivity and reduced roughness in comparison to other cathode geometries.

The inconsistencies in results from the PEG-based electrolyte are largely attributed to the reduced conductivity and increased viscosity compared to the acid-based electrolyte which impact the uniformity of electropolishing results. Conductivity measures how easily ions move in a solution, meaning that a larger conductivity facilitates ion mobility, which can commonly be the limiting factor during the electropolishing process [7, 62]. Additionally, several studies have shown that elevated temperatures further improve conductivity and thus, electropolishing effects [4, 7, 62, 70, 71, 88, 89]. Yang et al. claims that as electrolyte temperatures are increased, such as the increases noted in the acid-based electrolyte, viscosity decreases, resulting in a thinner diffusion layer on the anodic surface [62]. At too thin a diffusion layer, etching may occur [67, 90] which may be responsible for the dimpling characteristics consistently seen across optical images of all surfaces electropolished in the acid-based electrolyte. Such a phenomenon would explain why the acid-based electrolyte produced more consistent results when compared to a low-conductivity solution, such as the PEG-based electrolyte, where ion mobility is more restricted. However, since the process parameters, temperature, flow, etc., have not been fully optimized for the current setup, etching is still likely to have occurred.

The PEG-based electrolyte exhibits a significantly increased viscosity when compared to the acid-based electrolyte. Yang et al. asserts that an increased electrolyte viscosity causes a thicker diffusion layer to form on the anodic surface which is believed to control mass transport mechanisms in the electropolishing processes [7, 62]. A thicker diffusion layer further impedes ion mobility within the solution [62] and may be

responsible for the variation, optical streaking, non-uniform color, etc., across the anodic surfaces electropolished in the PEG-based electrolyte.

5.1.3: Roughness Reductions

The original surface roughness (S_a) of as-printed surfaces was reduced by approximately 40-75 % on all orientations after electropolishing in both electrolytes, except for samples polished with the flat cathode. The flat cathode consistently produced the highest surface roughness values, regardless of electrolyte or electrode spacing, and is not recommended as a suitable geometry for electropolishing T-shaped anodes due to lack of cathode proximity, which is essential for effective electropolishing [6, 8, 9, 11, 64]. Despite variations in reflectance and optical results, the front and back surfaces electropolished in the PEG-based electrolyte exhibited surface roughness approximately 1 μm lower than those electropolished in the acid-based electrolyte. This indicates that roughness results did not correlate with reflectance measurements, as acid-based samples exhibited higher reflectance values yet had higher surface roughness. Although reflectance values are a quick way to quantify surface brightness, they may not accurately indicate surface roughness, which is a major motivator for electropolishing.

Although the high viscosity and low conductivity of the PEG-based electrolyte made it challenging to obtain consistent results, these characteristics also explain why lower surface roughness was obtained compared to an acid-based electrolyte. Several studies recommend an electrolyte with low conductivity and high viscosity (such as ethylene glycol) to preferentially remove surface defects on an anode's surface [62, 66, 89]. Utilizing such electrolytes produces an increased voltage gradient (due to the increased viscosity and thicker diffusion layer) between peaks and valleys on the anodic

surface, resulting in preferential removal of peaks and thus, reduced surface roughness [62, 66, 89]. A study conducted by Abdel-Fattah and Loftis found that acidic electrolytes (such as those containing phosphoric acid) etched aluminum surfaces at a faster rate than ionic solutions (such as those based in choline chloride and ethylene glycol). The authors concluded that acidic electrolytes encouraged excessive hydrogen evolution which caused pitting on the anodic surface and recommended ionic electrolytes to produce favorable surface roughness [91]. The results found by Abdel-Fattah and Loftis are consistent with optical images of the present study of samples electropolished in the acid-based electrolyte, which demonstrated dimpling contributing to the increased surface roughness. It should be noted that although the PEG-based electrolyte produced lower surface roughness values for the present study, variations in the results should be considered. Due to physical limitations, roughness measurements were obtained from areas of the anodic surface where significant material removal was expected. Therefore, the lower roughness measurements observed with the PEG-based electrolyte may not be indicative of uniform roughness across the entire anode (i.e. the inner corners where less material removal is expected).

5.1.4: Impact of Initial Surface Roughness

The left and left-wall surface roughness values after electropolishing were approximately half of the front and back surfaces (after excluding the front cathode) which is attributed to initial surface roughness. Although the build-direction for the AM T-shaped anodes was chosen to promote similar starting roughness amongst all sides, there were significant discrepancies. Left and left-wall surfaces had an average starting roughness of 8.71 and 8.18 μm, respectively. Front and back surfaces had average

starting roughness of 10.89 and 11.81 μm, respectively, which is 2-3 μm higher than left and left-wall surfaces. It is well known that final surface roughness for electropolished parts can be dependent on initial surface roughness [1, 7]. In the present study, the PEG-based electrolyte demonstrated a higher sensitivity to initial surface roughness than the acid-based electrolyte. The PEG-based electrolyte was able to reduce the initial increased surface roughness of the front and back surfaces by approximately 7 and 6.5 μm on average, respectively. The left and left-wall surfaces, which exhibited a lower initial surface roughness, were only reduced by approximately 5.8 and 5.3 μm on average, respectively. However, the acid-based electrolyte reduced surface roughness by approximately 5.5 μm, on average, regardless of initial surface roughness values, indicating less sensitivity to initial surface roughness. The limitation from initial surface roughness in the electropolishing process is attributed to potential differences in the viscous layer, which controls the material removal mechanism [4, 7, 62]. Larger potential distributions, resulting from greater differences between peaks and valleys (i.e., larger surface roughness), create a greater electropolishing effect. Meanwhile, material removal rates on smoother surfaces are minimized due to the smaller differences in potential differences [7]. These results emphasize the significant influence of electropolishing parameters on results from the PEG-based electrolyte in comparison to the acid-based electrolyte and would suggest a lower conductivity, higher viscosity electrolyte may be a good approach to smoothing out the extremely rough as-printed surfaces.

5.2: Mass Changes and 2D Profilometry for Model and Experimental Results

5.2.1: Current Density Efficiencies

For the present study, a current density approximately seven times higher was applied to the acid-based electrolyte compared to the PEG-based electrolyte. It is well known in the electropolishing process that a higher current density results in higher material removal rates [7], which is corroborated by the results of the present study. However, the material removal rate of the acid-based electrolyte was only approximately twice that of the PEG-based electrolyte, despite the significantly higher applied current density. This is attributed to the higher current efficiency for the PEG-based electrolyte compared to the acid-based electrolyte, as outlined in several studies [7, 92, 93]. A study conducted by Haisch et al. tested the current efficiency of a NaCl-based electrolyte in an electrochemical machining process and found that it had current efficiency values of up to 115% at high current densities and up to 95% at low current densities (1 A/cm^2 and lower) [92]. Another study by Davis et al. investigated the current efficiency of a sulfuric acid (H_2SO_4) solution and found current efficiencies significantly lower than 50% for current densities from 0.1-0.3 A/cm^2 [93]. Similarly, an electropolishing study by Han and Fang comparing a NaCl-PEG-based electrolyte to an acid-based electrolyte attributed the higher material removal rates of the NaCl-PEG-based electrolyte to its higher current efficiency [6].

Several studies have attributed current efficiency losses to extensive hydrogen evolution [7, 91, 93-95]. A study conducted by Abdel-Fattah and Loftis compared electropolishing results between a conventional phosphoric acid electrolyte and a choline chloride, ethylene glycol electrolyte. The study concluded that hydrogen evolution was facilitated with the acid-based electrolyte due to faster polishing rates, resulting in pitting on the anodic surface [91]. A study by Gabe found that high current efficiencies (nearing

100 %) significantly reduced the occurrence of hydrogen evolution in electroplating practices [94]. Similarly, Han and Fang concluded that ionic solutions (such as those composed of choline chloride or ethylene glycol) exhibited negligible gas evolution due to their higher current efficiencies, making them more attractive than conventional electrolytes [7].

Overall, results from the COMSOL model aligned more closely with experimental results obtained from the more current efficient PEG-based electrolyte than with those from the acid-based electrolyte. The COMSOL model, based on primary current distributions, is inherently controlled by electrolyte conductivity and applied currents. The model physics are simplified through assumptions that neglect terms such as convection and diffusion. As a result, the model is not able to capture key differences between the two electrolytes, such as current efficiencies. Therefore, the model will predict that solutions such as the acid-based electrolyte, which have higher conductivity and applied current densities, will remove more material and act more aggressively than the PEG-based electrolyte, without accounting for the realistic differences in current efficiencies. The results imply the need to further develop the model physics to accommodate vital factors that more accurately represent real-world experiments.

5.2.2: Model Improvements

Future considerations for improving the COMSOL model physics include switching to tertiary current distributions. Tertiary current distributions include terms such as convection and diffusion which describe fluid flow and ion movements due to concentrations gradients, respectively. Such incorporations depict a more realistic representation of real-world phenomena, with fewer simplifications than primary current

distributions. The addition of fluid flow to the model would represent the continuous supply of refreshed electrolyte to the anodic surface, more closely resembling experimental conditions. Yang et al. explain the importance of electrolyte flow, as it helps to remove dissolved products from the anodic surface while decreasing the influence of bubbling and temperature rises often seen in electropolishing [62].

Future considerations also include introducing a pulsed current, similar to the one used experimentally. The direct current (DC) presently used in the model contributes to the excessive material removal rates observed in the results. It is well understood that direct currents selectively target sharp edges in comparison to recessed areas, causing an uneven current distribution on the anodic surface, as evidenced by model results in the present study. Yang et al. claim that a pulsed current encourages ion migration, resulting in more evenly distributed electropolishing effects compared to those achieved with DC [62].

Chapter 6 – Conclusion

In the present work, 316L stainless steel T-shaped anodes were fabricated using the LPBF AM technique. The effects of varying electrode spacings, cathode geometries, and electrolyte compositions on electropolishing results were analyzed. Anodes were characterized through optical imagery, surface roughness, reflectivity, mass, and profilometry measurements. The conclusions to take away from this work are:

1. The electropolishing process effectively reduced the original surface roughness (S_a) of as-printed surfaces by approximately 40-75 % on all orientations in both electrolyte compositions, excluding surfaces electropolished with the flat cathode geometry.
2. The acid-electrolyte demonstrated greater consistency in optical, roughness, reflectivity, and mass measurements whereas the PEG-based electrolyte exhibited greater sensitivity to electropolishing parameters. The standard deviation in surface roughness (S_a) was twice as high for the PEG-based electrolyte than the acid-based electrolyte. The PEG-based electrolyte showed an increased sensitivity to initial, as-printed surface roughness compared to the acid-based electrolyte.
3. When considering electrode spacing, there was a clear impact when the flat cathode was used in both electrolytes with a 20 mm spacing showing significantly less mass loss compared to the 2 mm spacing. Similar trends were seen for the flat cathode at 20 mm and roughness, most surfaces except the front showing higher roughness values than the 2 mm counterpart. The impact of electrode spacing on results obtained with the flat cathode are attributed to lack of cathode proximity.

4. The selective cathode produced the most consistent and uniform surfaces for the PEG-based electrolyte. The selective cathode consistently achieved low surface roughness, produced the brightest and most reflective surfaces, and created uniform surfaces as evidenced by optical images. In contrast, the flat cathode performed worst of all cathode geometries in the PEG-based electrolyte. The flat cathode produced high surface roughness values, low reflectivity, and inconsistencies in optical imagery.
5. Reflectivity measurements did not correlate with surface roughness (S_a) results. Despite variation and overall lower reflectance values, the PEG-based electrolyte produced surfaces approximately 1 μm smoother than the acid-based electrolyte. The reduction in surface roughness for the PEG-based electrolyte is attributed to its lower conductivity and higher viscosity, which produce an increased voltage gradient and a thicker diffusion layer. This results in the preferential removal of peaks, leading to an overall smoother surface. Although reflectance was a quick technique to quantify changes in surface brightness, it did not accurately indicate surface roughness.
6. Discrepancies between applied current densities and mass removal rates were discovered for the acid-based electrolyte. Several studies have demonstrated the higher current efficiency rates of electrolytes such as the PEG-based electrolyte [6, 92] when compared to current efficiency rates for electrolytes such as the acid-based electrolyte [93]. Consequently, the COMSOL model results for the acid-based electrolyte are overly exaggerated due to its higher conductivity and applied currents, without considering the real-world differences in current efficiencies.

These implications suggest the need to further develop the physics of the COMSOL model to reflect experimental conditions more accurately.

Future Considerations

Future considerations for this project include studying the impact of electrolyte flow and temperature on the electropolishing process. Present work has demonstrated that the PEG-based electrolyte appears to be more sensitive to electropolishing parameters such as electrode spacing and cathode geometry. However, future work aims to study and better control parameters such as electrolyte flow to determine the impact on electropolishing results, particularly in terms of electropolishing uniformity. Electrolyte flow is essential for maintaining uniform current distributions and removing dissolved products from the anodic surface [4, 6, 62]. In the present study, electrolyte temperature was not a controlled parameter. Future work looks to study the effects of electrolyte temperature which may influence diffusion rates and affect polishing quality [4, 6, 62, 70, 71].

Additionally, future works aims to further develop the physics of the developed COMSOL model to reflect experimental conditions more accurately. The incorporation of tertiary current distributions would provide a more realistic representation of convection and diffusion during the electropolishing process. Introducing a pulse current to the model will more accurately reflect experimental conditions and better depict ion migration. The integration of these elements will create an overall more realistic electropolishing model.

An automated optimization function for designing cathodes that uniformly remove material from the anode will also be investigated. While manual optimization has been shown to be possible, modifying the model to optimize the cathode shape itself would allow for a more quantifiable determination of cathode shape that will best fit the

ultimate goal of this project, being the uniform removal of materials from an anode. Improvements to the model via temperature and tertiary current distribution consideration will make the optimization of the cathode shape much more precise.

References

[1] E. S. Lee and T. H. Shin, "An evaluation of the machinability of nitinol shape memory alloy by electrochemical polishing," *Journal of mechanical science and technology,* vol. 25, pp. 963-969, 2011.

[2] J. Mingear, B. Zhang, D. Hartl, and A. Elwany, "Effect of process parameters and electropolishing on the surface roughness of interior channels in additively manufactured nickel-titanium shape memory alloy actuators," *Additive Manufacturing,* vol. 27, pp. 565-575, 2019.

[3] S. Chang *et al.*, "Highly effective smoothening of 3D-printed metal structures via overpotential electrochemical polishing," *Materials Research Letters,* vol. 7, no. 7, pp. 282-289, 2019.

[4] Z. Chaghazardi and R. Wüthrich, "Electropolishing of additive manufactured metal parts," *Journal of The Electrochemical Society,* vol. 169, no. 4, p. 043510, 2022.

[5] N. C. Ferreri, D. J. Savage, and M. Knezevic, "Non-acid, alcohol-based electropolishing enables high-quality electron backscatter diffraction characterization of titanium and its alloys: Application to pure Ti and Ti-6Al-4V," *Materials Characterization,* vol. 166, p. 110406, 2020.

[6] W. Han and F. Fang, "Eco-friendly NaCl-based electrolyte for electropolishing 316L stainless steel," *Journal of Manufacturing Processes,* vol. 58, pp. 1257-1269, 2020.

[7] W. Han and F. Fang, "Fundamental aspects and recent developments in electropolishing," *International Journal of Machine Tools and Manufacture,* vol. 139, pp. 1-23, 2019.

[8] A. Lassell, "The electropolishing of electron beam melting, additively manufactured TI6AL4V titanium: relevance, process parameters and surface finish," 2016.

[9] Z. Chaghazardi, L. Hof, and R. Wuthrich, "Electropolishing of inside surfaces of stainless steel tubing," *ECS Transactions,* vol. 97, no. 7, p. 523, 2020.

[10] M. Shen, C. Kang, and F. Fang, "Material removal characteristics of various surface features on selective laser melted 316L stainless steel during electropolishing," *Journal of Manufacturing Processes,* vol. 79, pp. 639-653, 2022.

[11] S. Zaki, N. Zhang, and M. D. Gilchrist, "Electropolishing and shaping of micro-scale metallic features," *Micromachines,* vol. 13, no. 3, p. 468, 2022.

[12] M. E. Lynch, K. Williams, M. Cabrera, and T. Beccuti, "Surface finishing of additively manufactured IN718 lattices by electrochemical machining," *The International Journal of Advanced Manufacturing Technology,* vol. 113, no. 3, pp. 967-984, 2021.

[13] T. D. Ngo, A. Kashani, G. Imbalzano, K. T. Nguyen, and D. Hui, "Additive manufacturing (3D printing): A review of materials, methods, applications and challenges," *Composites Part B: Engineering,* vol. 143, pp. 172-196, 2018.

[14] G. Pyka, G. Kerckhofs, I. Papantoniou, M. Speirs, J. Schrooten, and M. Wevers, "Surface roughness and morphology customization of additive manufactured open porous Ti6Al4V structures," *Materials,* vol. 6, no. 10, pp. 4737-4757, 2013.

[15] G. Strano, L. Hao, R. M. Everson, and K. E. Evans, "Surface roughness analysis, modelling and prediction in selective laser melting," *Journal of Materials Processing Technology,* vol. 213, no. 4, pp. 589-597, 2013.

[16] W. J. Sames, F. List, S. Pannala, R. R. Dehoff, and S. S. Babu, "The metallurgy and processing science of metal additive manufacturing," *International materials reviews,* vol. 61, no. 5, pp. 315-360, 2016.

[17] M. A. Melia, J. G. Duran, J. R. Koepke, D. J. Saiz, B. H. Jared, and E. J. Schindelholz, "How build angle and post-processing impact roughness and corrosion of additively manufactured 316L stainless steel," *npj Materials Degradation,* vol. 4, no. 1, p. 21, 2020.

[18] F. Cabanettes *et al.*, "Topography of as built surfaces generated in metal additive manufacturing: A multi scale analysis from form to roughness," *Precision Engineering,* vol. 52, pp. 249-265, 2018.

[19] J. C. Fox, S. P. Moylan, and B. M. Lane, "Effect of process parameters on the surface roughness of overhanging structures in laser powder bed fusion additive manufacturing," *Procedia Cirp,* vol. 45, pp. 131-134, 2016.

[20] B. Whip, L. Sheridan, and J. Gockel, "The effect of primary processing parameters on surface roughness in laser powder bed additive manufacturing," *The International Journal of Advanced Manufacturing Technology,* vol. 103, pp. 4411-4422, 2019.

[21] G. E. Bean, D. B. Witkin, T. D. McLouth, D. N. Patel, and R. J. Zaldivar, "Effect of laser focus shift on surface quality and density of Inconel 718 parts produced via selective laser melting," *Additive Manufacturing,* vol. 22, pp. 207-215, 2018.

[22] I. Koutiri, E. Pessard, P. Peyre, O. Amlou, and T. De Terris, "Influence of SLM process parameters on the surface finish, porosity rate and fatigue behavior of as-built Inconel 625 parts," *Journal of Materials Processing Technology,* vol. 255, pp. 536-546, 2018.

[23] S. Liu and Y. C. Shin, "Additive manufacturing of Ti6Al4V alloy: A review," *Materials & Design,* vol. 164, p. 107552, 2019.

[24] M. Benedetti *et al.*, "The effect of post-sintering treatments on the fatigue and biological behavior of Ti-6Al-4V ELI parts made by selective laser melting," *Journal of the mechanical behavior of biomedical materials,* vol. 71, pp. 295-306, 2017.

[25] B. Vayssette, N. Saintier, C. Brugger, M. Elmay, and E. Pessard, "Surface roughness of Ti-6Al-4V parts obtained by SLM and EBM: Effect on the High Cycle Fatigue life," *Procedia engineering,* vol. 213, pp. 89-97, 2018.

[26] H. Rafi, N. Karthik, H. Gong, T. L. Starr, and B. E. Stucker, "Microstructures and mechanical properties of Ti6Al4V parts fabricated by selective laser melting and electron beam melting," *Journal of materials engineering and performance,* vol. 22, pp. 3872-3883, 2013.

[27] M. Fousová, D. Vojtěch, K. Doubrava, M. Daniel, and C.-F. Lin, "Influence of inherent surface and internal defects on mechanical properties of additively manufactured Ti6Al4V alloy: Comparison between selective laser melting and electron beam melting," *Materials,* vol. 11, no. 4, p. 537, 2018.

[28] E. Santos, K. Osakada, M. Shiomi, Y. Kitamura, and F. Abe, "Microstructure and mechanical properties of pure titanium models fabricated by selective laser melting," *Proceedings of the institution of mechanical engineers, part c: journal of mechanical engineering science,* vol. 218, no. 7, pp. 711-719, 2004.

[29] M. Montemor, M. Ferreira, N. Hakiki, and M. D. C. Belo, "Chemical composition and electronic structure of the oxide films formed on 316L stainless steel and nickel based alloys in high temperature aqueous environments," *Corrosion Science,* vol. 42, no. 9, pp. 1635-1650, 2000.

[30] B. Evgeny, T. Hughes, and D. Eskin, "Effect of surface roughness on corrosion behaviour of low carbon steel in inhibited 4 M hydrochloric acid under laminar and turbulent flow conditions," *Corrosion Science,* vol. 103, pp. 196-205, 2016.

[31] L. R. Hilbert, D. Bagge-Ravn, J. Kold, and L. Gram, "Influence of surface roughness of stainless steel on microbial adhesion and corrosion resistance," *International biodeterioration & biodegradation,* vol. 52, no. 3, pp. 175-185, 2003.

[32] W. Wang, K. Yung, H. Choy, T. Xiao, and Z. Cai, "Effects of laser polishing on surface microstructure and corrosion resistance of additive manufactured CoCr alloys," *Applied Surface Science,* vol. 443, pp. 167-175, 2018.

[33] J. J. de Damborenea *et al.*, "Functionalization of Ti6Al4V scaffolds produced by direct metal laser for biomedical applications," *Materials & Design,* vol. 83, pp. 6-13, 2015.

[34] R. Melchers and R. Jeffrey, "Surface “Roughness” effect on marine immersion corrosion of mild steel," *Corrosion,* vol. 60, no. 7, pp. 697-703, 2004.

[35] M. A. Melia, J. G. Duran, J. M. Taylor, F. Presuel-Moreno, R. F. Schaller, and E. J. Schindelholz, "Marine atmospheric corrosion of additively manufactured stainless steels," *Corrosion,* vol. 77, no. 9, pp. 1003-1013, 2021.

[36] G. Sander *et al.*, "On the corrosion and metastable pitting characteristics of 316L stainless steel produced by selective laser melting," *Journal of the electrochemical society,* vol. 164, no. 6, p. C250, 2017.

[37] M. Cabrini *et al.*, "Evaluation of corrosion resistance of Al–10Si–Mg alloy obtained by means of Direct Metal Laser Sintering," *Journal of Materials Processing Technology,* vol. 231, pp. 326-335, 2016.

[38] E. Wycisk, A. Solbach, S. Siddique, D. Herzog, F. Walther, and C. Emmelmann, "Effects of defects in laser additive manufactured Ti-6Al-4V on fatigue properties," *Physics Procedia,* vol. 56, pp. 371-378, 2014.

[39] P. Maiya and D. Busch, "Effect of surface roughness on low-cycle fatigue behavior of type 304 stainless steel," *Metallurgical Transactions A,* vol. 6, pp. 1761-1766, 1975.

[40] S. Leuders *et al.*, "On the mechanical behaviour of titanium alloy TiAl6V4 manufactured by selective laser melting: Fatigue resistance and crack growth performance," *International journal of fatigue,* vol. 48, pp. 300-307, 2013.

[41] K. S. Chan, M. Koike, R. L. Mason, and T. Okabe, "Fatigue life of titanium alloys fabricated by additive layer manufacturing techniques for dental implants," *Metallurgical and Materials Transactions A,* vol. 44, pp. 1010-1022, 2013.

[42] P. Edwards and M. Ramulu, "Fatigue performance evaluation of selective laser melted Ti–6Al–4V," *Materials Science and Engineering: A,* vol. 598, pp. 327-337, 2014.

[43] E. Wycisk, S. Siddique, D. Herzog, F. Walther, and C. Emmelmann, "Fatigue performance of laser additive manufactured Ti–6Al–4V in very high cycle fatigue regime up to 109 cycles," *Frontiers in Materials,* vol. 2, p. 72, 2015.

[44] E. Brandl, U. Heckenberger, V. Holzinger, and D. Buchbinder, "Additive manufactured AlSi10Mg samples using Selective Laser Melting (SLM): Microstructure, high cycle fatigue, and fracture behavior," *Materials & Design,* vol. 34, pp. 159-169, 2012.

[45] B. Song, S. Dong, Q. Liu, H. Liao, and C. Coddet, "Vacuum heat treatment of iron parts produced by selective laser melting: Microstructure, residual stress and tensile behavior," *Materials & Design (1980-2015),* vol. 54, pp. 727-733, 2014.

[46] J. T. Staley Jr, M. Tiryakioğlu, and J. Campbell, "The effect of hot isostatic pressing (HIP) on the fatigue life of A206-T71 aluminum castings," *Materials Science and Engineering: A,* vol. 465, no. 1-2, pp. 136-145, 2007.

[47] X. Shui, K. Yamanaka, M. Mori, Y. Nagata, K. Kurita, and A. Chiba, "Effects of post-processing on cyclic fatigue response of a titanium alloy additively manufactured by electron beam melting," *Materials Science and Engineering: A,* vol. 680, pp. 239-248, 2017.

[48] W. Kniffka, M. Eichmann, and G. Witt, *Rapid. Tech–International Trade Show & Conference for Additive Manufacturing: Proceedings of the 13th Rapid. Tech Conference Erfurt, Germany, 14–16 June 2016*. Carl Hanser Verlag GmbH Co KG, 2016.

[49] C. Qiu, N. J. Adkins, and M. M. Attallah, "Microstructure and tensile properties of selectively laser-melted and of HIPed laser-melted Ti–6Al–4V," *Materials Science and Engineering: A,* vol. 578, pp. 230-239, 2013.

[50] M. Pattabi and K. Ramakrishna, "Effect of mechanical cutting and polishing on the shape memory transformation behavior of NiTi alloy," *Materials Science and Engineering: A,* vol. 486, no. 1-2, pp. 14-18, 2008.

[51] P. Tyagi *et al.*, "Roughness reduction of additively manufactured steel by electropolishing," *The International Journal of Advanced Manufacturing Technology,* vol. 106, pp. 1337-1344, 2020.

[52] U. S. Kim and J. W. Park, "High-quality surface finishing of industrial three-dimensional metal additive manufacturing using electrochemical polishing," *International Journal of Precision Engineering and Manufacturing-Green Technology,* vol. 6, pp. 11-21, 2019.

[53] Y.-C. Wu, C.-N. Kuo, Y.-C. Chung, C.-H. Ng, and J. C. Huang, "Effects of electropolishing on mechanical properties and bio-corrosion of Ti6Al4V fabricated by electron beam melting additive manufacturing," *Materials,* vol. 12, no. 9, p. 1466, 2019.

[54] Z. Zhang, Z. Shi, Y. Du, Z. Yu, L. Guo, and D. Guo, "A novel approach of chemical mechanical polishing for a titanium alloy using an environment-friendly slurry," *Applied Surface Science,* vol. 427, pp. 409-415, 2018.

[55] D. Brent, T. A. Saunders, F. Garcia Moreno, and P. Tyagi, "Taguchi design of experiment for the optimization of electrochemical polishing of metal additive manufacturing components," in *ASME International Mechanical Engineering Congress and Exposition*, 2016, vol. 50527: American Society of Mechanical Engineers, p. V002T02A014.

[56] L. S. Andrade, S. C. Xavier, R. C. Rocha-Filho, N. Bocchi, and S. R. Biaggio, "Electropolishing of AISI-304 stainless steel using an oxidizing solution

originally used for electrochemical coloration," *Electrochimica Acta,* vol. 50, no. 13, pp. 2623-2627, 2005.

[57] P. Szymczyk-Ziółkowska *et al.*, "The impact of EBM-manufactured Ti6Al4V ELI alloy surface modifications on cytotoxicity toward eukaryotic cells and microbial biofilm formation," *Materials,* vol. 13, no. 12, p. 2822, 2020.

[58] C. Rotty, M.-L. Doche, A. Mandroyan, J.-Y. Hihn, G. Montavon, and V. Moutarlier, "Comparison of electropolishing behaviours of TSC, ALM and cast 316L stainless steel in H3PO4/H2SO4," *Surfaces and Interfaces,* vol. 6, pp. 170-176, 2017.

[59] S. Habibzadeh, L. Li, D. Shum-Tim, E. C. Davis, and S. Omanovic, "Electrochemical polishing as a 316L stainless steel surface treatment method: Towards the improvement of biocompatibility," *Corrosion science,* vol. 87, pp. 89-100, 2014.

[60] J. W. Park and D. W. Lee, "Pulse electrochemical polishing for microrecesses based on a coulostatic analysis," *The International Journal of Advanced Manufacturing Technology,* vol. 40, pp. 742-748, 2009.

[61] A. G. Demir and B. Previtali, "Additive manufacturing of cardiovascular CoCr stents by selective laser melting," *Materials & Design,* vol. 119, pp. 338-350, 2017.

[62] G. Yang, B. Wang, K. Tawfiq, H. Wei, S. Zhou, and G. Chen, "Electropolishing of surfaces: theory and applications," *Surface Engineering,* vol. 33, no. 2, pp. 149-166, 2017.

[63] H. Aihara, *Surface and biocompatibility study of electropolished Co-Cr alloy L605*. San Jose State University, 2009.

[64] E.-S. Lee, "Machining characteristics of the electropolishing of stainless steel (STS316L)," *The International Journal of Advanced Manufacturing Technology,* vol. 16, pp. 591-599, 2000.

[65] H. Ramasawmy and L. Blunt, "Investigation of the effect of electrochemical polishing on EDM surfaces," *The International Journal of Advanced Manufacturing Technology,* vol. 31, pp. 1135-1147, 2007.

[66] D. Landolt, "Fundamental aspects of electropolishing," *Electrochimica Acta,* vol. 32, no. 1, pp. 1-11, 1987.

[67] P. Jacquet, "The mechanism of electrolytic polishing of Copper," *CR Acad Sci,* vol. 202, p. 402, 1936.

[68] R. Grimm, A. West, and D. Landolt, "AC impedance study of anodically formed salt films on iron in chloride solution," *Journal of the electrochemical society,* vol. 139, no. 6, p. 1622, 1992.

[69] M. Matlosz, S. Magaino, and D. Landolt, "Impedance analysis of a model mechanism for acceptor-limited electropolishing," *Journal of the electrochemical society,* vol. 141, no. 2, p. 410, 1994.

[70] S. Chen, G. Tu, and C. Huang, "The electrochemical polishing behavior of porous austenitic stainless steel (AISI 316L) in phosphoric-sulfuric mixed acids," *Surface and Coatings Technology,* vol. 200, no. 7, pp. 2065-2071, 2005.

[71] D. Ma, S. Li, and C. Liang, "Electropolishing of high-purity aluminium in perchloric acid and ethanol solutions," *Corrosion Science,* vol. 51, no. 4, pp. 713-718, 2009.

[72] C. Wagner, "Contribution to the theory of electropolishing," *Journal of the electrochemical society,* vol. 101, no. 5, p. 225, 1954.

[73] M. Haidopoulos, S. Turgeon, C. Sarra-Bournet, G. Laroche, and D. Mantovani, "Development of an optimized electrochemical process for subsequent coating of 316 stainless steel for stent applications," *Journal of Materials Science: Materials in Medicine,* vol. 17, pp. 647-657, 2006.

[74] K. Alrbaey, D. I. Wimpenny, A. Al-Barzinjy, and A. Moroz, "Electropolishing of re-melted SLM stainless steel 316L parts using deep eutectic solvents: 3× 3 full factorial design," *Journal of Materials Engineering and Performance,* vol. 25, pp. 2836-2846, 2016.

[75] M. Inman, E. Taylor, A. Lozano-Morales, and L. Zardiackas, "Electropolishing and throughmask electroetching of Nitinol stents and other materials in an aqueous electrolyte," in *Medical Device Materials VI: Proceedings from the Materials and Processes for Medical Devices Conference:(MPMD 2011)*, 2013: ASM International, p. 31.

[76] M. Datta and D. Landolt, "Fundamental aspects and applications of electrochemical microfabrication," *Electrochimica acta,* vol. 45, no. 15-16, pp. 2535-2558, 2000.

[77] V. Urlea and V. Brailovski, "Electropolishing and electropolishing-related allowances for powder bed selectively laser-melted Ti-6Al-4V alloy components," *Journal of Materials Processing Technology,* vol. 242, pp. 1-11, 2017.

[78] W. Han and F.-Z. Fang, "Investigation of electropolishing characteristics of tungsten in eco-friendly sodium hydroxide aqueous solution," *Advances in Manufacturing,* vol. 8, no. 3, pp. 265-278, 2020.

[79] H. Zhao, J. V. Humbeeck, J. Sohier, and I. D. Scheerder, "Electrochemical polishing of 316L stainless steel slotted tube coronary stents," *Journal of Materials science: materials in medicine,* vol. 13, pp. 911-916, 2002.

[80] V. Finazzi, A. G. Demir, C. A. Biffi, F. Migliavacca, L. Petrini, and B. Previtali, "Design and functional testing of a novel balloon-expandable cardiovascular stent in CoCr alloy produced by selective laser melting," *Journal of Manufacturing Processes,* vol. 55, pp. 161-173, 2020.

[81] U. Ali, H. Fayazfar, F. Ahmed, and E. Toyserkani, "Internal surface roughness enhancement of parts made by laser powder-bed fusion additive manufacturing," *Vacuum,* vol. 177, p. 109314, 2020.

[82] F. Eozénou, S. Berry, C. Antoine, Y. Gasser, J.-P. Charrier, and B. Malki, "Aging of the HF-H 2 SO 4 electrolyte used for the electropolishing of niobium superconducting radio frequency cavities: Origins and cure," *Physical Review Special Topics—Accelerators and Beams,* vol. 13, no. 8, p. 083501, 2010.

[83] N. P. Aryan, H. Kaim, and A. Rothermel, *Stimulation and recording electrodes for neural prostheses*. Springer, 2015.

[84] T. Pérez, C. P. de León, F. C. Walsh, and J. L. Nava, "Simulation of current distribution along a planar electrode under turbulent flow conditions in a laboratory filter-press flow cell," *Electrochimica Acta,* vol. 154, pp. 352-360, 2015.

[85] K. Popov, B. Grgur, and S. S. Djokić, *Fundamental aspects of electrometallurgy*. Springer, 2007.

[86] COMSOL. Electrochemistry Module User's Guide (Version 5.6)

[87] P. Pendyala, M. Bobji, and G. Madras, "Evolution of surface roughness during electropolishing," *Tribology Letters,* vol. 55, pp. 93-101, 2014.

[88] M. Hernando, P. J. Núñez, E. García Plaza, and R. Trujillo, "Effect of electrolyte on the surface smoothness obtained by electropolishing of stainless steel," in *Materials Science Forum*, 2012, vol. 713: Trans Tech Publ, pp. 55-60.

[89] W. J. M. Tegart, "The electrolytic and chemical polishing of metals in research and industry," *(No Title),* 1959.

[90] A. Hickling and J. Higgins, "The rate-determining stage in the anodic dissolution of metals," *Transactions of the IMF,* vol. 29, no. 1, pp. 274-301, 1952.

[91] T. M. Abdel-Fattah and J. D. Loftis, "Comparison of Electropolishing of Aluminum in a Deep Eutectic Medium and Acidic Electrolyte," *Molecules,* vol. 25, no. 23, p. 5712, 2020.

[92] T. Haisch and E. Mittemeijer, "Electrochemical machining: the role of steel microstructure in high-rate anodic dissolution," *Jom,* vol. 54, pp. 38-41, 2002.

[93] J. R. Davis, J. C. Baygents, and J. Farrell, "Effect of current density and sulfuric acid concentration on persulfuric acid generation by boron-doped diamond film anodes," *Journal of Applied Electrochemistry,* vol. 44, pp. 841-848, 2014.

[94] D. Gabe, "The role of hydrogen in metal electrodeposition processes," *Journal of applied electrochemistry,* vol. 27, no. 8, pp. 908-915, 1997.

[95] A. P. Abbott, G. Capper, K. J. McKenzie, and K. S. Ryder, "Voltammetric and impedance studies of the electropolishing of type 316 stainless steel in a choline chloride based ionic liquid," *Electrochimica Acta,* vol. 51, no. 21, pp. 4420-4425, 2006.